Forme d'onda con modulazione di fase

Pierfrancesco Lombardo

Forme d'onda con codifica di fase

$$s_0(t) = \frac{1}{\sqrt{N\tau_p}} \sum_{n=0}^{N-1} s_{0n}(t - n \cdot \tau_p)$$

$$s_{0n}(t) = e^{j\phi_n}\, rect_{\tau_p}(t - \frac{\tau_p}{2}) = \begin{cases} e^{j\phi_n}, & 0 \le t \le \tau_p \\ 0, & altrove \end{cases}$$

Barker
Frank
P3 e P4
P(n,k)

- **Codici bi-fase**:
  - facili da implementare
  - permettono buon controllo dei lobi laterali
  - non forte tolleranza alla frequenza Doppler

- **Codici poli-fase**:
  - tendono ad avere migliore tolleranza alla frequenza Doppler
  - tendono a permettere un miglior controllo dei lobi laterali

Codici Binari

- **La fase della portante ad RF commuta fra due valori di fase distanti di 180°**

  Può essere descritta usando sequenze di +1 e -1:

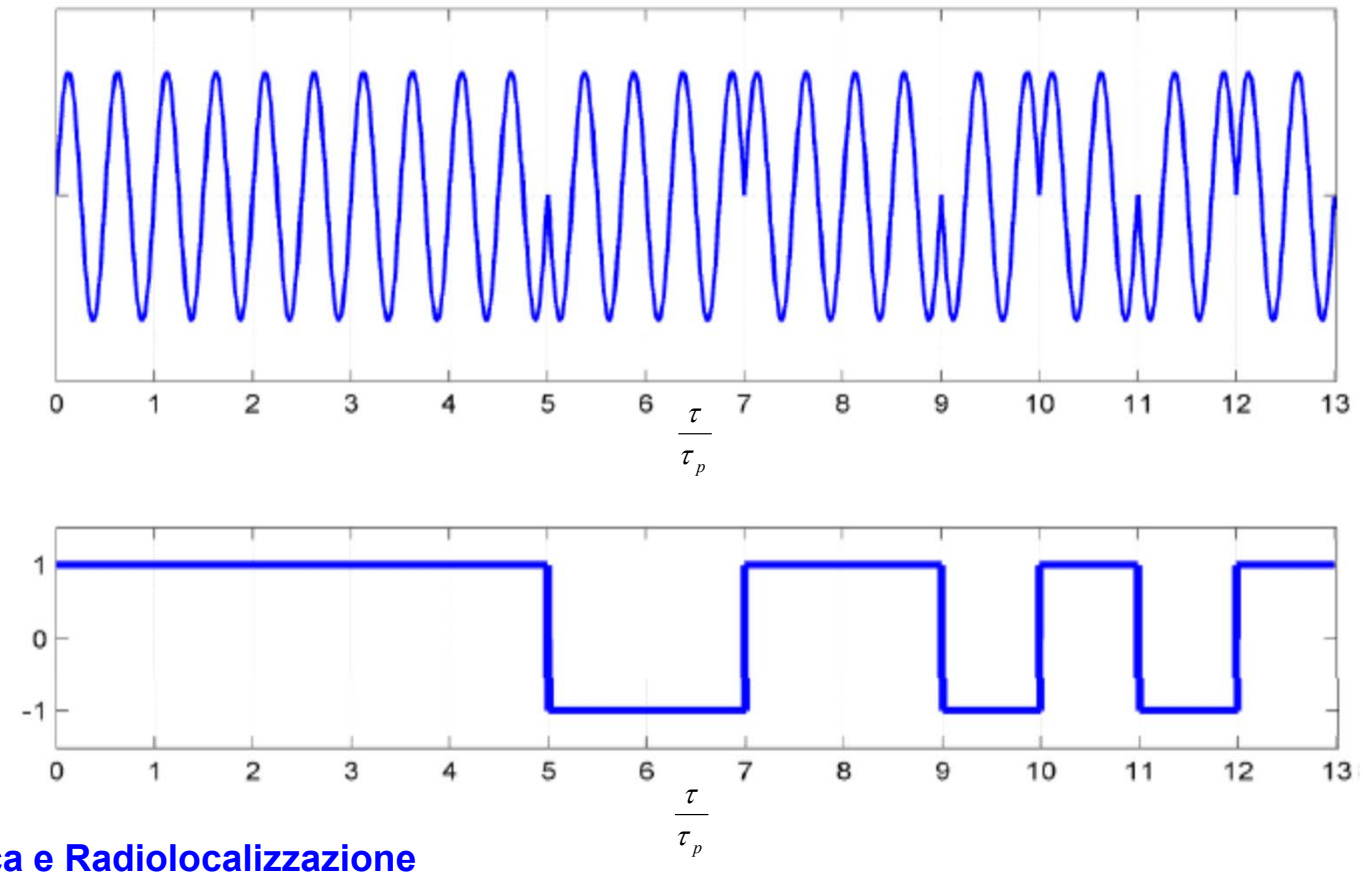

Codici di Barker

Sono codici binari di lunghezza N, caratterizzati da Funzione di AutoCorrelazione (ACF) con lobi laterali in modulo ≤ 1/N

- Esistono solo poche sequenze con queste caratteristiche:

Lunghezza N	codice	PSR (dB)	ISLR (dB)
2	+ -	6,0	3,0
2	++	6,0	3,0
3	++-	9,5	6,5
3	+-+	9,5	6,5
4	++-+	12,0	6,0
4	+++-	12,0	6,0
5	+++-+	14,0	8,0
7	+++--+-	16,9	9,1
11	+++---+--+-	20,8	10,8
13	+++++--++-+-+	22,3	11,5

Calcolo ACF del codice di Barker da 7

Table 8.3 The Autocorrelation Sequence of a Barker Code of Length 7

$\{u_n\}$	+	+	+	−	−	+	−						
$\{u^*_{N-n+1}\}$													
−	−	−	−	+	+	−	+						
+		+	+	+	−	−	+	−					
−			−	−	−	+	+	−	+				
−				−	−	−	+	+	−	+			
+					+	+	+	−	−	+	−		
+						+	+	+	−	−	+	−	
+							+	+	+	−	−	+	−
Output sequence	−1	0	−1	0	−1	0	+7	0	−1	0	−1	0	−1

Da N. Levanon, “Radar Principles”

ACF del codice di Barker da 13

Rispetto ad impulso non modulato τ_p:

- Energia trasmessa BT=n=13 volte superiore
- risoluzione in tempo uguale

- risoluzione in Doppler BT=n=13 volte superiore
- (zona cieca BT=n=13 volte più larga)

Rispetto ad impulso non modulato $T=n\tau_p$:

- Energia trasmessa uguale

- risoluzione in tempo BT=n=13 volte migliore
- risoluzione in Doppler uguale

- (zona cieca uguale)

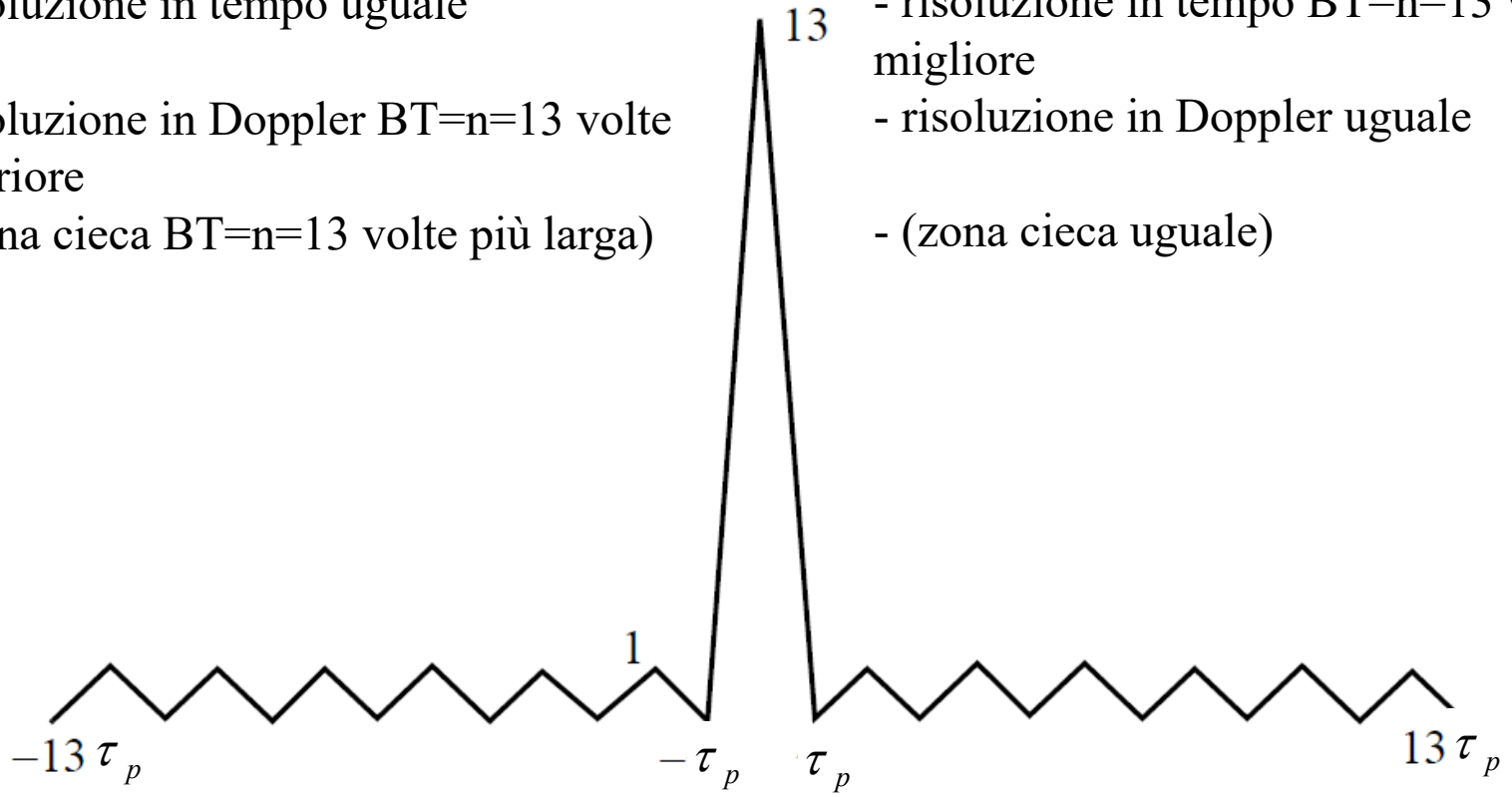

Codici di Barker innestati

- Si possono innestare codici di barker fra loro:
- Esempio di ACF per combinazione di Barker 13 con Baker 3

1 1 1 1 1 -1 -1 1 1 -1 1 -1 1 1 1 1 1 -1 -1 1 1 -1 1 -1 1 -1 -1 -1 -1 -1 -1 1 1 -1 -1 1 -1 1 -1

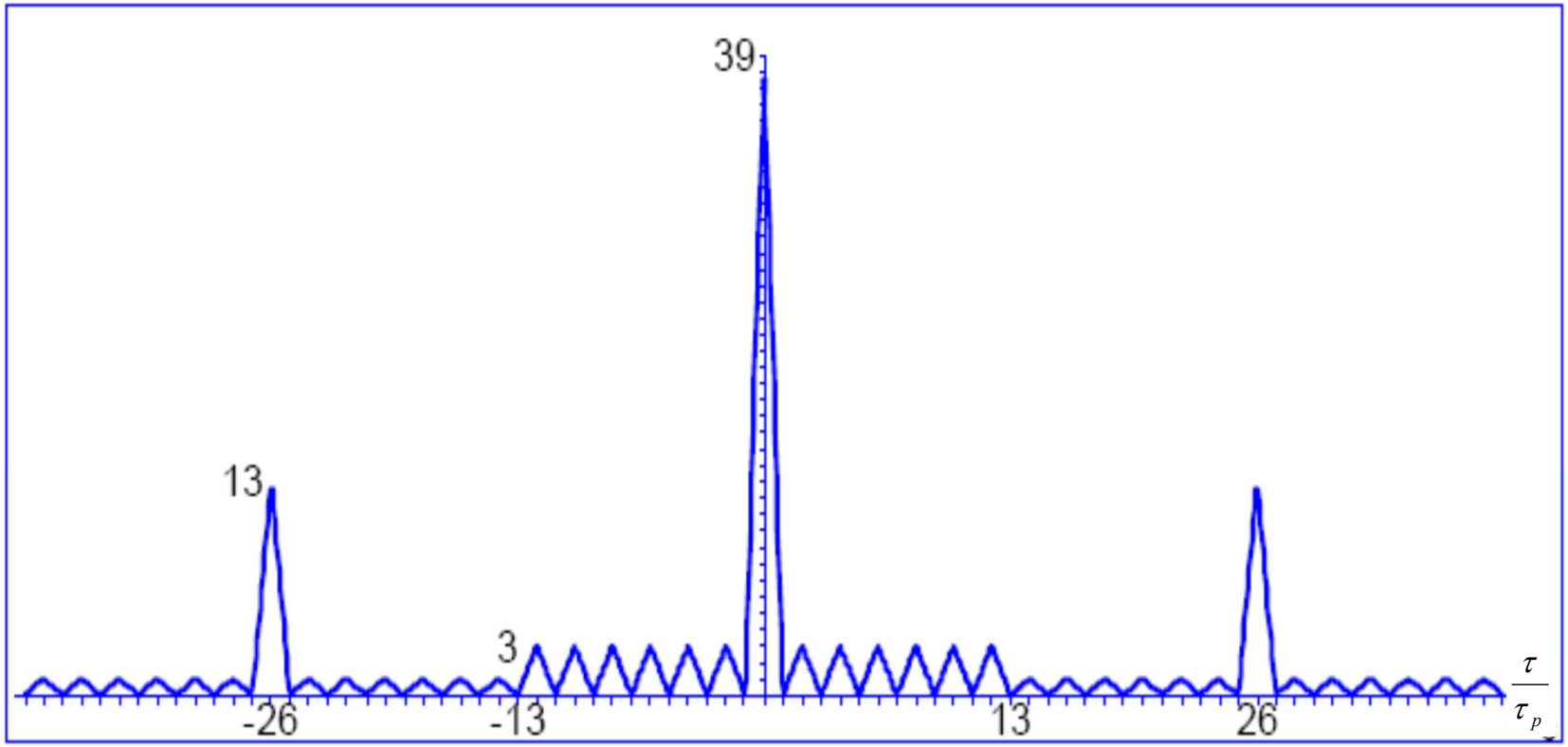

Codici di Barker Polifase

- Usare valori di fase generici (non binari) può portare a lobi più bassi e sequenze lunghe
- Il lobo laterale più lontano dal picco vale sempre 1 (sia per codici binary che polifase)
- Le sequenze polifase con PSLR massimo (escluso il lobo laterale esterno) sono chiamate **sequenze di barker generalizzate** o **sequenze di Barker Polifase**

Codici di Barker Polifase

- **Caso 1:** valori di fase pari alla radice k-esima dell'unità
  (es: *k=2 codici di Barker, k=6 sextic Barker codes).*

- **Caso 2:** senza restrizione sui valori di fase quantizzati utilizzabili
  (sequenze note per valori di $M \leq 36$)

Codici di Barker Polifase (I)

Espressione in forma normalizzata:

i primi due elementi di ogni codice valgono 0 e non sono riportati in tabella.

M	Peak sidelobe	Phase values [°]
4	0.5	104 313
5	0.77	73 225.3 90.6
6	1	58.2 175.9 354.1 234.2
7	0.522	106.4 93 316.7 60.5 270.7
8	0.662	72.1 28.6 294.3 151.7 251.2 63.3
9	0.430	38.7 41.5 270.2 215.1 40.5 160.7 334.3[el]
10	0.832	60.2 132.1 142.8 18.3 10.7 230.8 22.9 242.9
11	0.892	34.1 259 266.5 327.9 158.4 13.7 22.7 221.5 94.5
12	0.908	104.8 163 170.9 344.3 241 185.5 282.2 147.6 209 78.7
13	0.721	115.8 114.8 248.4 213.4 123.1 154.9 140.2 12.7 149.6 303.5 121.6
14	0.968	66.8 133.5 202.2 100.4 37.5 235.8 167.2 86 168.7 33.5 143.1 13.3
15	0.805	17.8 5.5 5.4 142.4 212 298.1 123.9 91.6 1.3 206 314.2 156.5 23.9
16	0.933	26.5 38.5 97.3 49.4 305.8 286.5 197 65.7 241.3 137.5 319.1 47.9 178.5 303
17	0.733	5.3 18.5 278.4 307.6 67.3 149 207.5 70.6 301.2 282.8 137.3 6.5 120.5 327.9 186
18		(?)
19	0.980	53.3 24.7 90 79.2 232.5 8 331.4 99 240 318.4 159.8 307.8 161.3 137.1 31.8 338.2 217
20	0.979	99.1 125.8 233.1 251.4 133.9 144 354.8 304.5 192.1 302.5 219.5 161.7 283.8 145.4 250.2 106.1 228.4 107

Codici di Barker Polifase (II)

Espressione in forma normalizzata:

i primi due elementi di ogni codice valgono 0 e non sono riportati in tabella.

22	0.995	23.8 53.7 82.1 74.5 349.3 265 314 247.2 147.2 74.6 285.7 160.2 335.4 78.5 317.2 148.4 248.6 344.3 87.8 208.7
23	0.912	7.4 276 286.4 253.9 256.7 351.7 58.4 60.2 226.3 353.1 100.5 168.6 41 208.5 347.8 219.2 125.9 349.7 315.3 182.1 56.3
24	0.997	5 316.4 257.1 216.5 202.4 319 311.1 356.9 296.8 111.2 36.1 280.8 136.9 10.1 115.7 259.2 134.3 268.0 28.0 142.3 208.4 333.8
25	0.936	81.9 65 316.3 273.1 326.3 339.8 62.7 18.8 270.5 198 98.8 126.6 206.5 350.7 105.9 270.8 295.4 162.3 334.2 155.5 339.8 147.7 4.4
26	0.879	51.3 117.1 138.2 265.4 267 175.4 117.8 260.2 200 136.1 154.2 179 75.8 341 187.4 307 194.4 92.5 190.2 17.2 110 250.3 38.7 199.7
27	0.985	10.6 21.9 28.7 324.7 308.4 280.6 118.4 99.2 112.2 284.5 200.6 313.8 116.3 326.7 184.8 53.4 8.8 193.9 97.1 240.9 335.3 103 228.6 332 93
28	0.950	46.9 84.3 166.3 145.7 199.8 105.1 116.6 58.7 109.7 325.9 24.3 189.9 21.4 196.2 58.8 326.5 129.2 259 306.7 123.5 111.2 312.7 298.5 173.8 97.9 327.8
29	0.871	6.9 318.2 239.9 264.7 239.2 160.4 301.5 327.5 18.7 319.7 84.9 108.6 224.1 6.3 31.4 184 167.8 89.9 325.2 227.5 145.4 329.9 91.6 263.7 94 252.9 59.6
30	0.998	33.1 34.6 33.7 11.9 300.1 281.5 26.5 54.2 155.6 211.9 231.6 134.4 76 317.7 275.8 67.6 299 184.6 72.6 153.8 6.6 262.6 94.1 242.8 359.1 149.7 306.4 71.5
31	0.935	28.4 117.7 165.1 236.5 308.7 305 236.5 216.4 327.4 279.5 211.3 247.2 192 95.4 17 273 52.8 331.1 224 303.7 147.2 21.7 245.6 29.3 145.5 297.1 62.4 190.8 7.8
32	0.996	13.5 16.5 90.5 110 95 60.5 333 307 289 281.5 85.5 164 248.5 335 171.5 76 64 221.5 298 110 37 272.5 179.5 19.5 179 288 82.5 292 133 329.5
33	0.990	143 153.5 339 332.5 180.5 133.5 19 108.5 166 216.5 225.5 227.5 318.5 238.5 184.5 226 141.5 113.5 75 36 185.5 327 226.5 108.5 302.5 116.5 273 350 188 356.5 164.5
34	0.997	11 1 307 245 200 184 231 293 300 348 45 227 247 57 335 1 127 249 68 91 315 221 57 116 238 58 287 127 273 127 5 216
35	0.999	93.2 65.4 166.4 132.4 344.1 279.4 337.6 301.3 197.6 56.2 36.8 9.2 325.8 334.3 24.4 157.8 291.1 301.1 148.4 112.9 141.3 296.6 128.7 125.4 341.4 129.9 244.6 73.8 321.5 157.6 300.7 107.5 254.4
36	0.969	82 118 228 228 58 60 154 108 20 234 212 262 236 196 220 116 12 226 178 122 126 76 266 114 256 108 320 100 266 30 124 246 60 186

ACF del codice di Barker Polifase con M=15

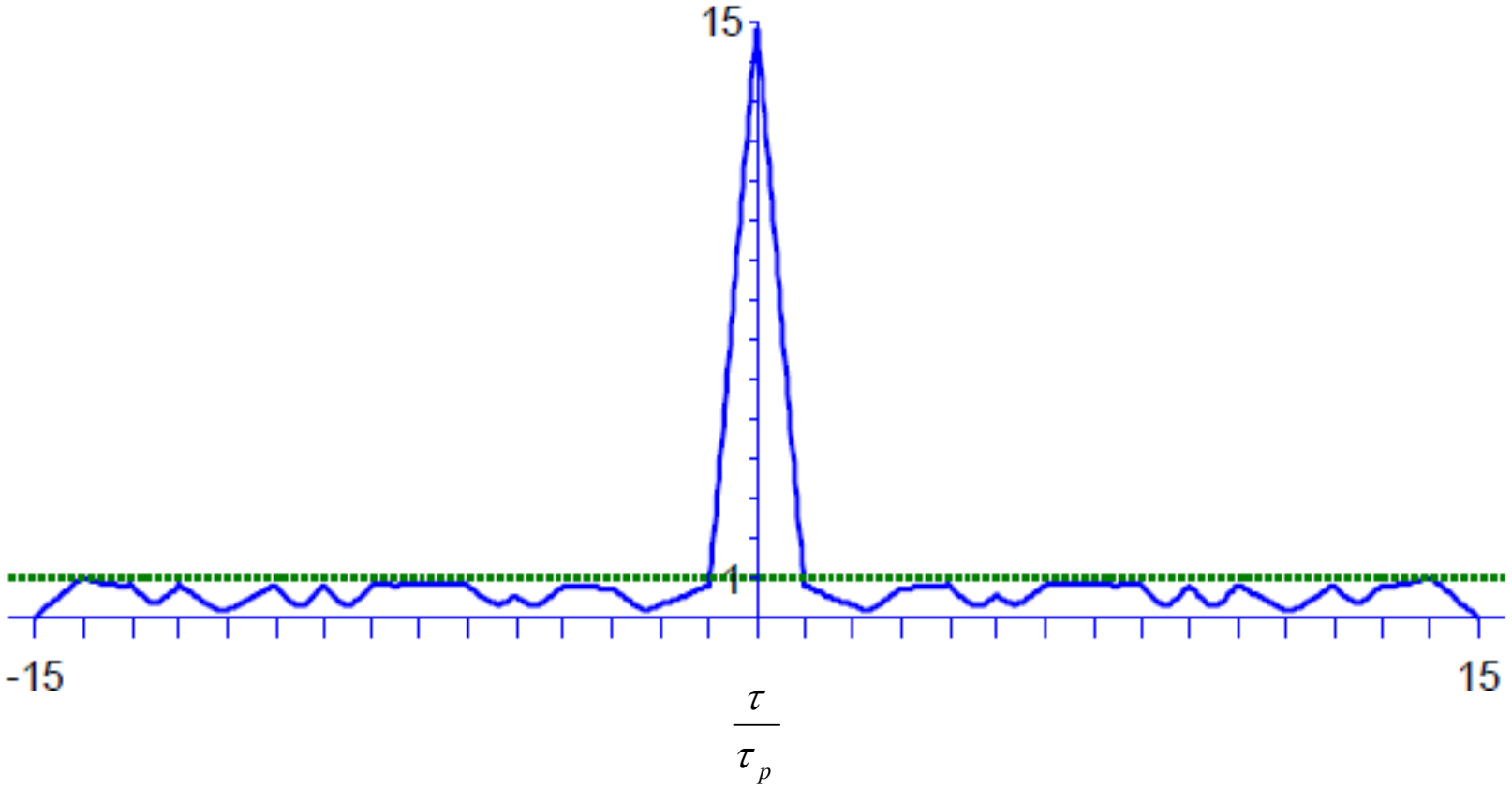

Codici binari con PSL massimo (I)

M	PSL	Sample code
6	2	110100
8	2	10010111
9	2	011010111
10	2	0101100111
12	2	100101110111
14	2	01010010000011
15	2	001100000101011
16	2	0110100001110111
17	2	00111011101001011
18	2	011001000011110101
19	2	1011011101110001111
20	2	01010001100000011011
21	2	101101011101110000011
22	3	001110011011010101111111
23	3	011100011111110101001001
24	3	011001001010111111100011
25	2	100100101010000001110011 1
26	3	100011100000001010111011001
27	3	010010110111011101110000111
28	2	100011110001000100010010110 1
29	3	101100100101010000000111001 11
30	3	100011000101010010010000001111
31	3	010101001001001100011000000 1111
32	3	000000011110010110101010110011 00
33	3	011001100101010100101100001111111
34	3	110011001111111111000011010010101 01
35	3	000000001111100101101010101100110011
36	3	001100110001010010100000100000111110

G. Coxson &
J Russo,
IEEE Trans
on AES
Jan 2005

Codici binari con PSL massimo (II)

37	3	00101011101000010011101101111100111 10
38	3	000000001111000011010010101010011001 10
39	3	00100110011010100001011111011110011110 0
40	3	00100010001000111101110000111010010110 10
41	3	00011100011101010010100100000001101100100
42	3	00010001000100011110111000011101001011010 0
43	3	00000000101101100101010110011001110000111 00
44	3	00001111111101100111011001011001010101101 0111
45	3	00010101011110000110011000110110110111111110110
46	3	00001111000000110011110111110110110010101010110
47	3	00001101001101010011111101000010100011001100010000
48	3	00010101011010110110000011110011001001111111110011
49	4	00000100101010101111101100011111001111001000110111 11
50	4	00001001011000011000111010101111000010011001101111
51	3	00011100011111111000100011001000100101010010010011
52	4	00001001010001011010111000001111001100100100001101111
53	4	00001001100101010101001111111110001101001011000110111 11
54	4	00001001100110101000101000000101001011001111100011011 11
55	4	00001001100001001101010101000011110001100100100011011 11
56	4	00001001100110111010101011001011010001111011110001101111
57	4	00001001001101000101010001110110101100010001111100011011 11
58	4	00001000111100111001010100010111001001111011010110011011 11
59	4	00001001001110100111000000100101000101000011101111000110111
60	4	00001010101110000110111110000110010010111001100100101001011 11
61	4	00000010110110100010011000100110001111001111010100011010100 00
62	4	00000000101101011001100110001101001100101100000111010001010000
63	4	00001001100111101011010001001000111000101100101011111000110111 11
64	4	01000000100100000101000101110100111100110001100100011011111000010
65	4	00000001011011100000010110000011011001101111001110010101000101000 0
66	4	00000001101001101101000101010001110011100111111000100101011010000010
67	4	01000000101000001101100100110101011000111101001000010011100110000 10
68	4	00000000100111100100100111100011011001100010101010000111010100101000 0
69	4	00010011011111111011011000001001101010000011101000001000110001111000010101
70	4	01101000010011001110110100111000110000100100111111011011101010101111110

Lobi laterali

Quanto è importante ridurre i lobi laterali?

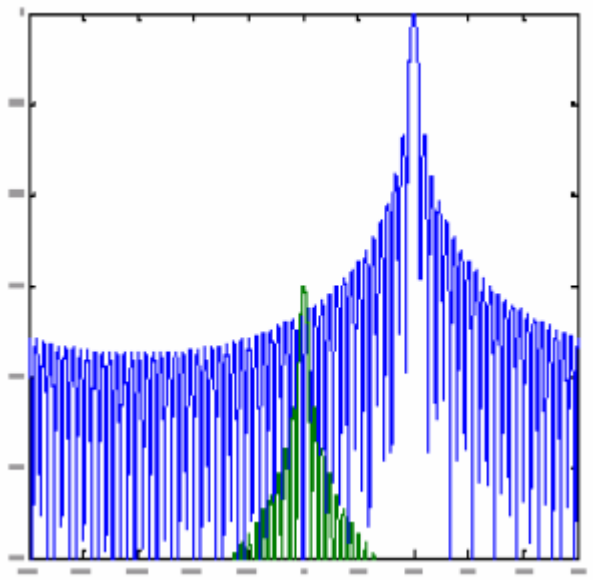

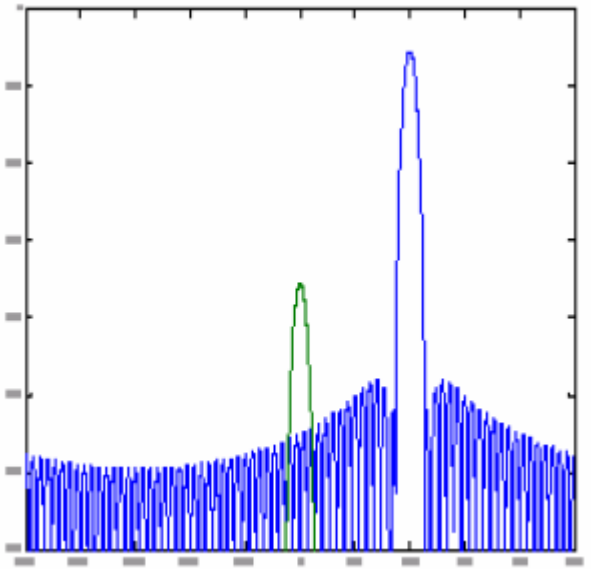

Senza pesatura con pesatura di Hamming

Codici con ACF ideale

- **E' possibile trovare una sequenza di impulsi con ACF ideale (lobi laterali a zero) ?**

NO

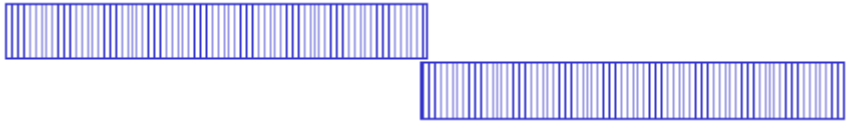

- Ci si può avvicinare di più a tale ACF usando i codici di Huffman, che richiedono modulazione di ampiezza e fase

Codice Polifase di Frank (I)

- **Usando M valori di fase**
- **Numero di elementi $N=M^2$**
- **Costruito dalle righe della matrice quadrata:**

$$\phi_{pq} = \frac{2\pi}{M}(p-1)(q-1) \qquad p,q = 1, \cdots, M$$

- **Per N=16**

$$\phi_{pq} \quad \begin{bmatrix} 0 & 0 & 0 & 0 \\ 0 & \pi/2 & \pi & 3\pi/2 \\ 0 & \pi & 2\pi & 3\pi \\ 0 & 3\pi/2 & 3\pi & 9\pi/2 \end{bmatrix} \qquad s_{0\,pq} = e^{j\phi_{pq}} \quad \begin{bmatrix} 1 & 1 & 1 & 1 \\ 1 & j & -1 & -j \\ 1 & -1 & 1 & -1 \\ 1 & -j & -1 & j \end{bmatrix}$$

Codice Polifase di Frank (II)

$$\phi_m = \frac{2\pi}{M}(m-1)\left(\left\lfloor \frac{m}{M} \right\rfloor - 1\right) \qquad m = 1, \cdots, M^2$$

Forma di quantizzazione di un segnale chirp

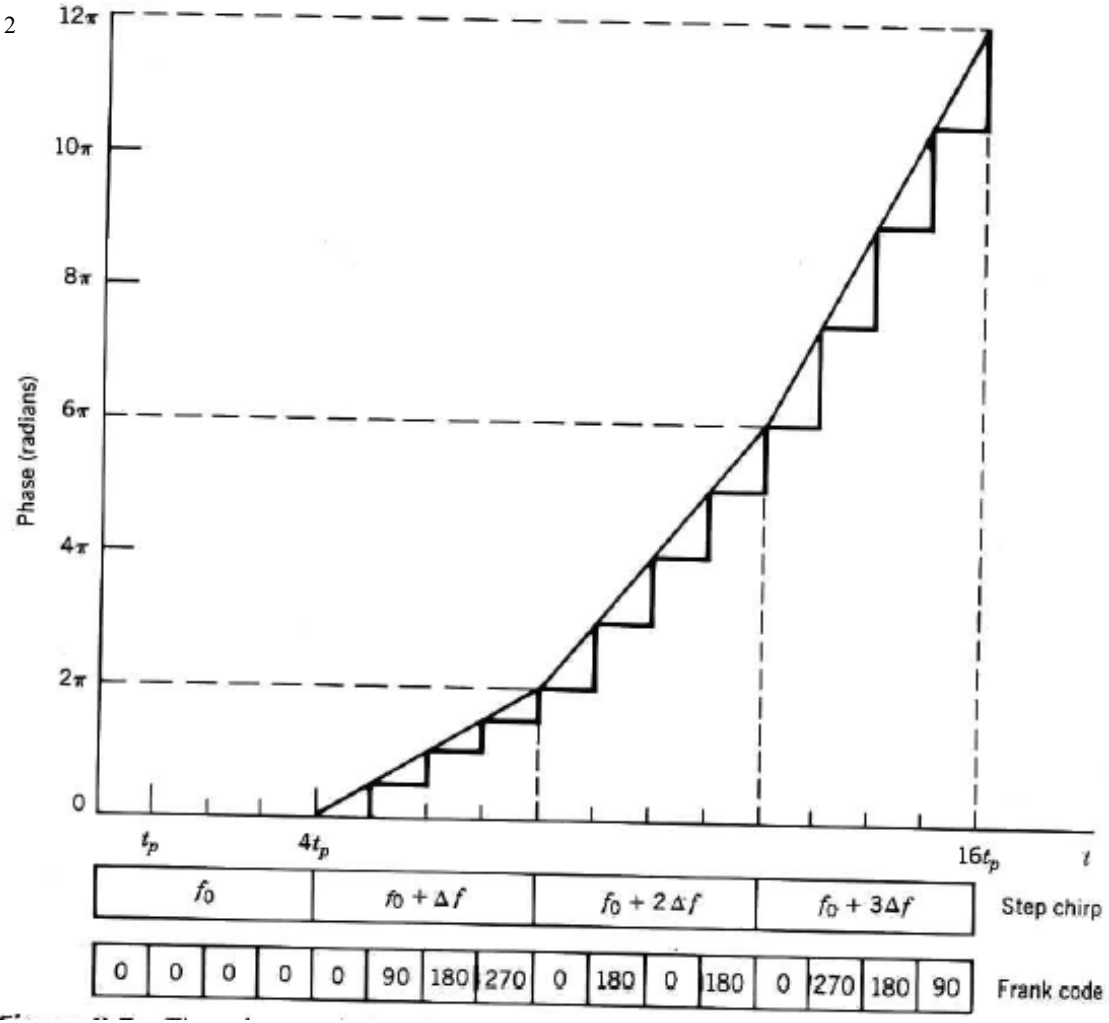

Codice Polifase di Frank (III)

Table 8.5 The Autocorrelation Sequence of a 16-Bit Frank Code

$\{u_n\}$ / $\{u^*_{-n+1}\}$	1	1	1	1	1	j	−1	$-j$	1	−1	1	−1	1	$-j$	−1	j
$-j$	$-j$	$-j$	$-j$	$-j$	$-j$	1	j	−1	$-j$	j	$-j$	j	$-j$	−1	j	1
−1		−1	−1	−1	−1	−1	$-j$	1	j	−1	1	−1	1	−1	j	1
j			j	j	j	j	j	−1	$-j$	1	j	$-j$	j	−1	j	1
1				1	1	1	1	1	j	−1	$-j$	1	−1	1	−1	1
−1					−1	−1	−1	−1	−1	$-j$	1	j	−1	1	−1	1
1						1	1	1	1	1	j	−1	$-j$	1	−1	1
−1							−1	−1	−1	−1	−1	$-j$	1	j	−1	1
1								1	1	1	1	1	j	−1	$-j$	1
j									j	j	j	j	j	−1	$-j$	1
−1										−1	−1	−1	−1	−1	$-j$	1
$-j$											$-j$	$-j$	$-j$	$-j$	$-j$	1
1												1	1	1	1	1
1													1	1	1	1
1														1	1	1
1															1	1
1																1
Output seq.	$-j$	−1	−1	0	−1	1	j	0	j	−1	1	0	1	1	$-j$	16
		$-j$				$+j$				$+j$				$-j$		

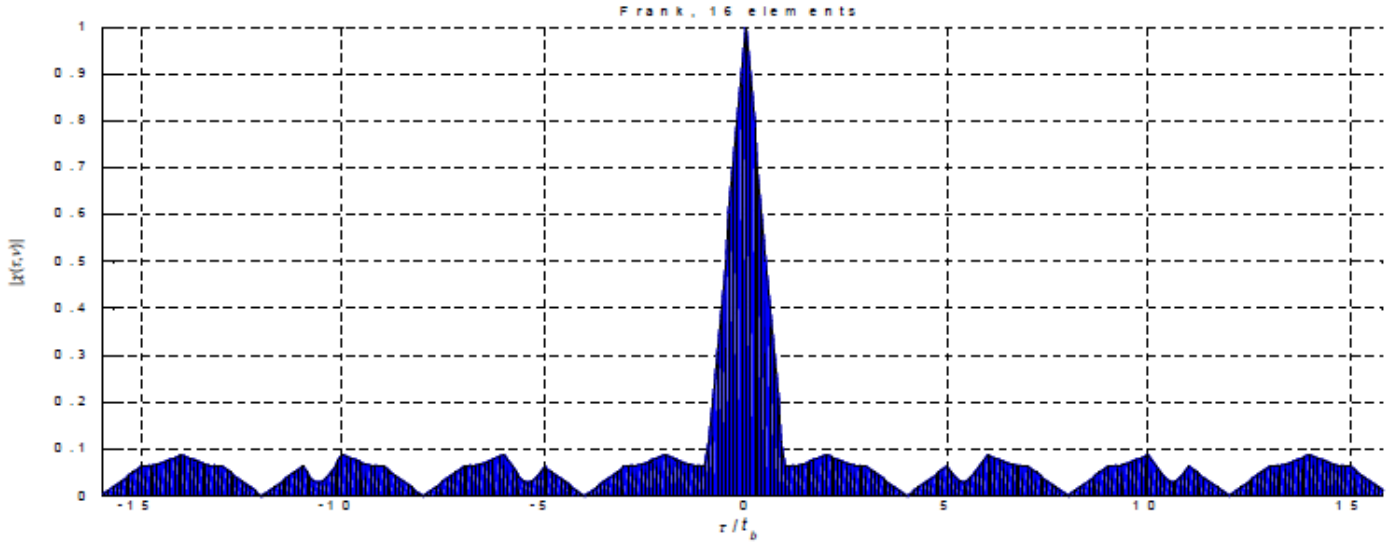

Radiotecnica e

Codice Polifase di Frank (IV)

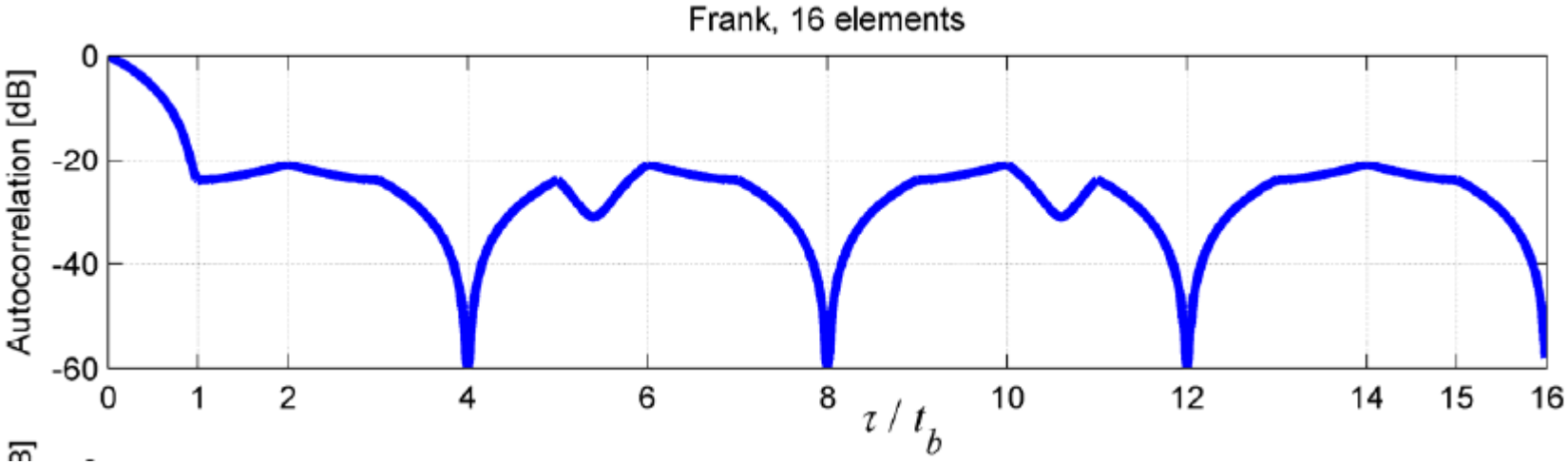

Per N= 16 $PSR = \frac{16}{\sqrt{2}} = 8\sqrt{2} = 11{,}3 \quad (21dB)$ *(peggiore di Barker)*

Per N grande $PSR = \pi\sqrt{N} = \pi\ M \quad \Rightarrow 9.94 + 10 * \log_{10}(N)$

(N=100 ~30 dB)

Codici Polifase P3 e P4 (I)

Codice P3

per M pari $\phi_m = \frac{\pi}{M}(m-1)^2 \quad m = 1, \cdots, M$

per M dispari $\phi_m = \frac{\pi}{M}(m-1)m \quad m = 1, \cdots, M$

Codice P4

$$\phi_m = \frac{\pi}{M}(m-1)^2 - \pi\,(m-1) \quad m = 1, \cdots, M$$

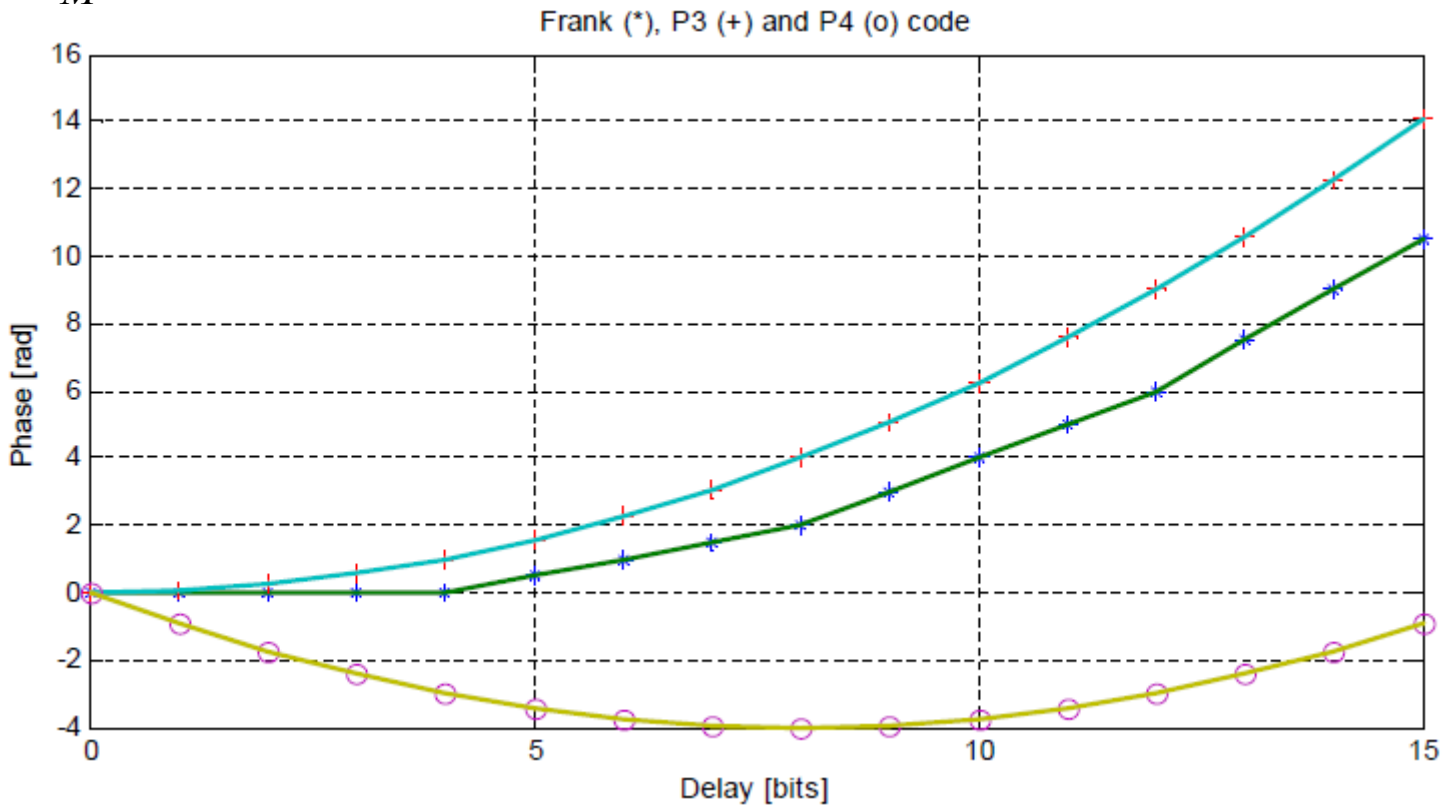

Radiotecnica e Ra

Codici Polifase P3 e P4 (III)

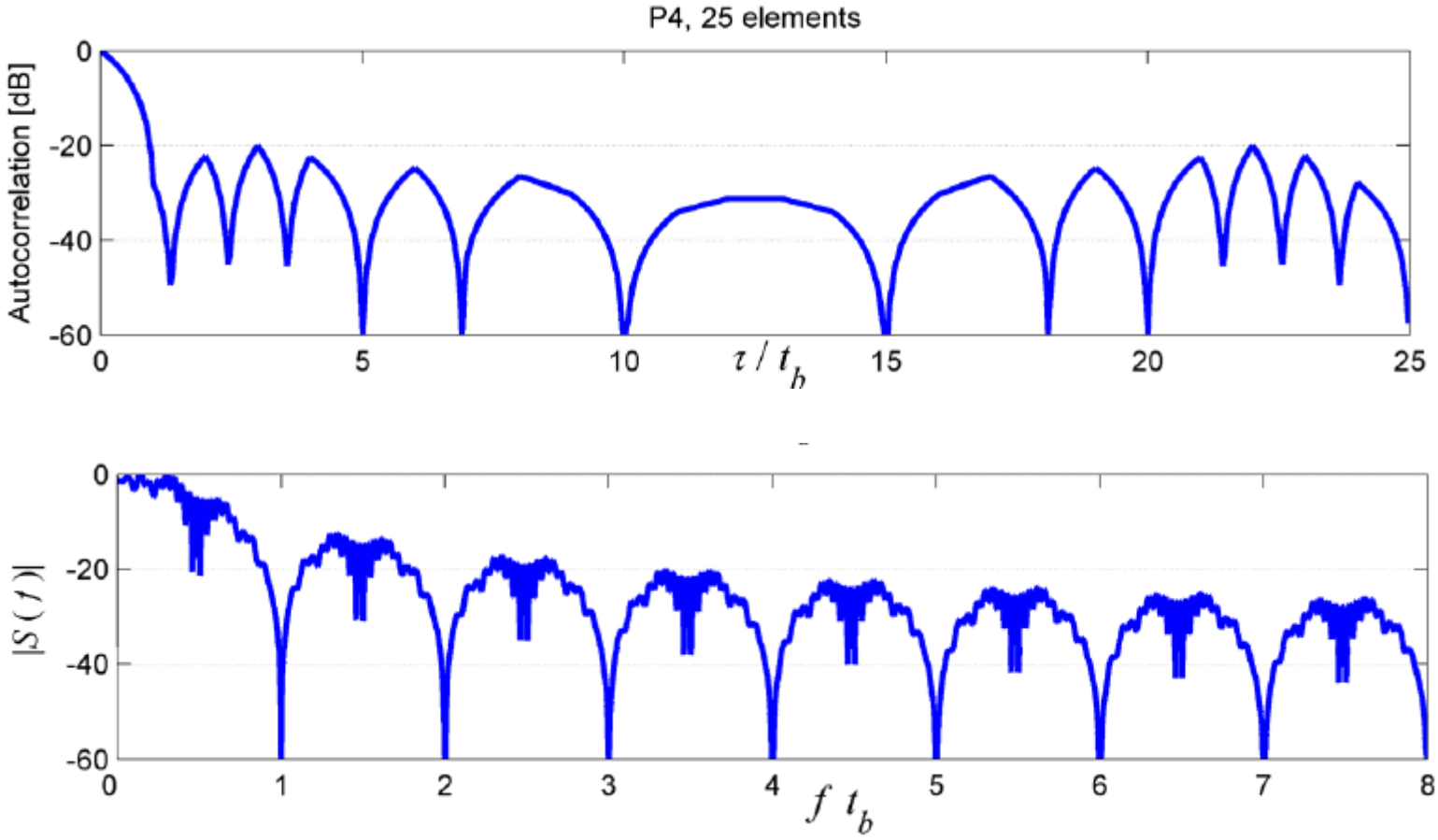

Filtro adattato al singolo impulso

- Per $\tau_p < T/2$:

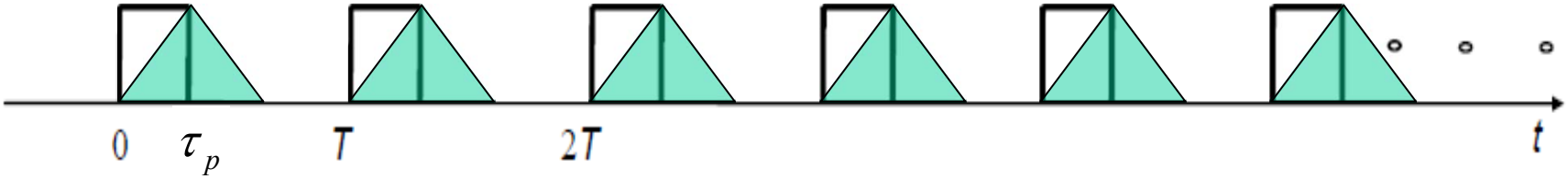

- Per $\tau_p = T$:

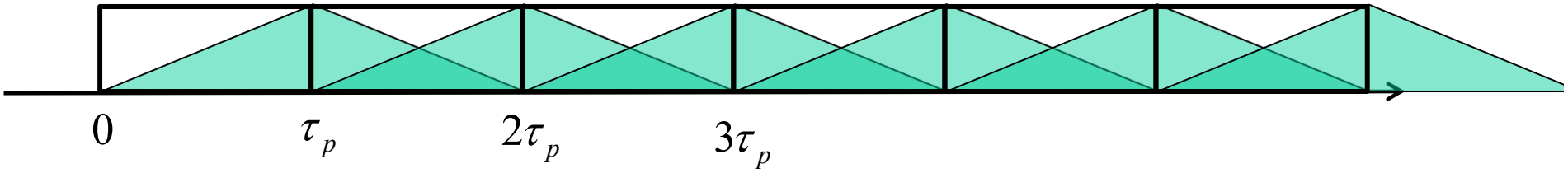

- **Periodic Ambiguity Function**

$$\left|\chi_P(\tau,\nu)\right| = \left| \int_0^T s_0(t)\; s_{0P}^*(t+\tau)\; e^{j2\pi\nu t} dt \right|$$

$$\left|\chi_P(\tau,\nu)\right| = \left| \int_0^T s_0(t) \sum_{n=-\infty}^{\infty} s_0^*(t - n\cdot T + \tau)\; e^{j2\pi\nu t} dt \right|$$

PAF del Barker 4

1	1	-1	1	1	1	-1	1	1	1	-1	1	1	1	-1	1	1	1	-1	1
1	1	-1	1																
	1	1	-1	1															
		1	1	-1	1														
			1	1	-1	1													
				1	1	-1	1												
					1	1	-1	1											
						1	1	-1	1										
							1	1	-1	1									

---

4 0 0 0 4 0 0

Autocorrelazione periodica perfetta!

PAF dei codici di Frank

Frank 16

Autocorrelazione periodica perfetta!

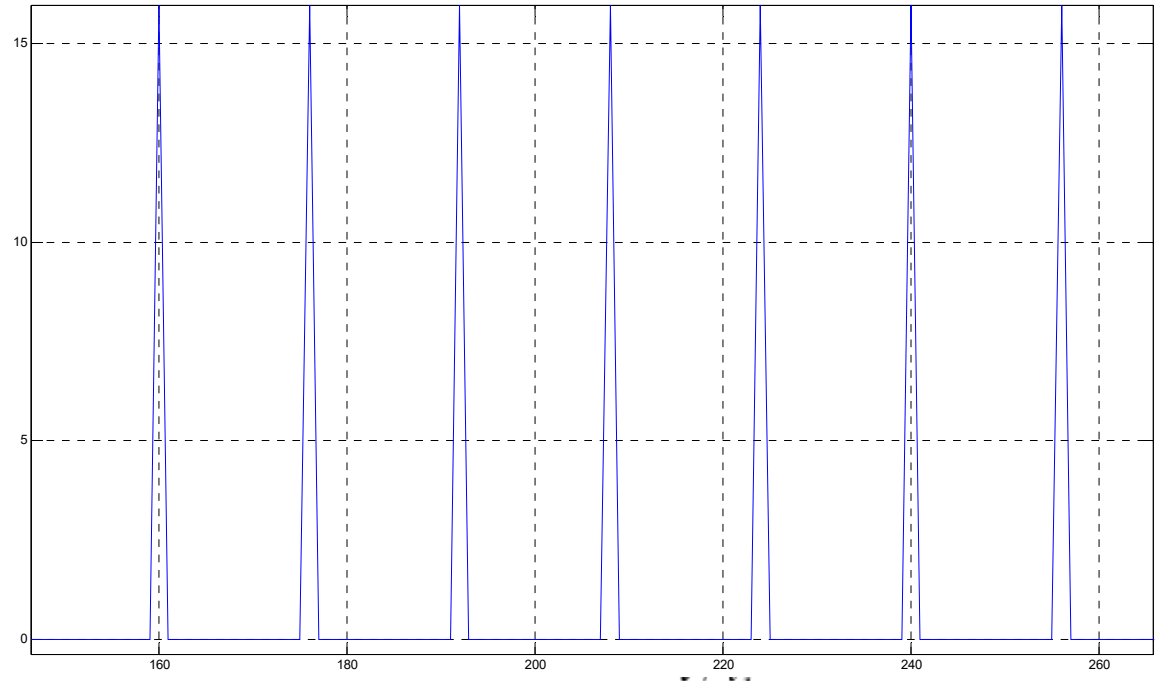

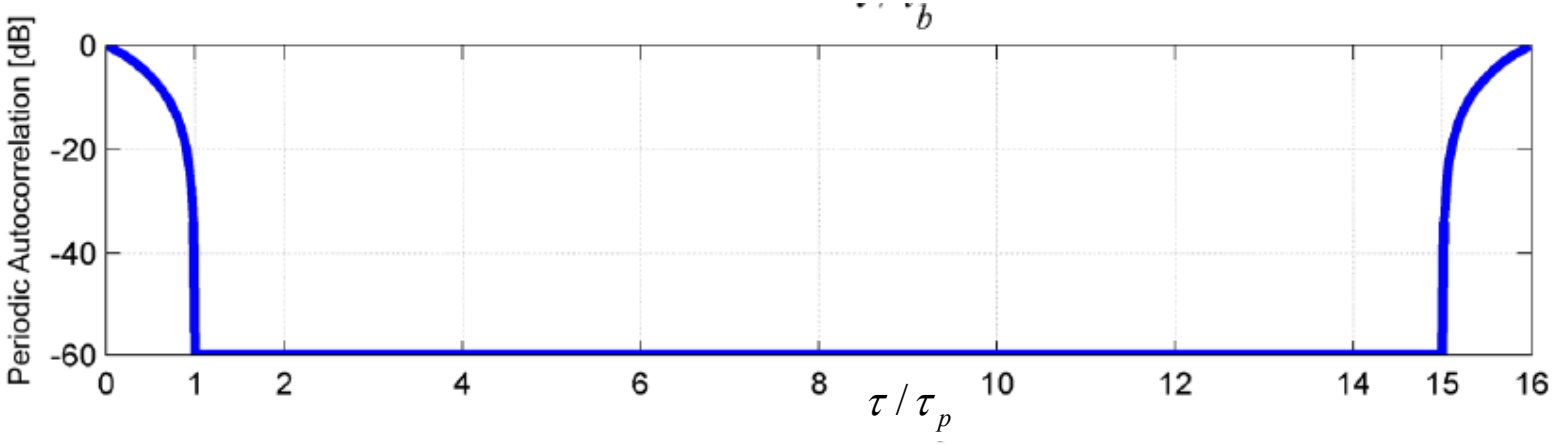

PAF dei codici P4

P4 da 25 elementi

Autocorrelazione periodica perfetta!

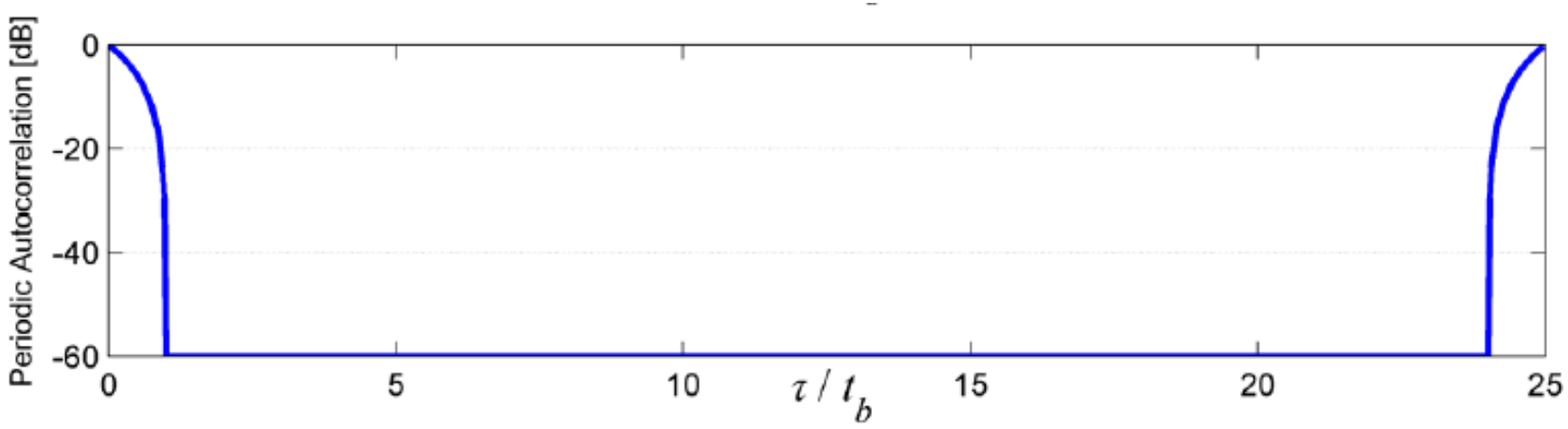

CHIRP: linear frequency modulated signal

MAXIMUM RADAR RANGE

$$R_{max} = \sqrt[4]{\frac{E_T G^2 \lambda^2 \sigma}{(4\pi)^3 K T_0 F S_a}} \qquad \text{Con } E_T = P_p T$$

RANGE RESOLUTION

$$R_d = \frac{cT}{2}$$

CHIRP: LINEAR FREQUENCY MODULATION

$$s(t) = e^{j2\pi\left(f_p t + \frac{B}{T}\cdot\frac{t^2}{2}\right)} \mathrm{rect}_T(t)$$

B chirp bandwidth
T transmitted pulse length
f_p (residual) carrier frequency

- CHIRP (long pulse with phase coding): has the power properties of the long pulse and the resolution properties of the short pulse.

- Phase coding → waveform compression by means of matched filtering

CHIRP: Time domain waveform (I)

$$s(t) = e^{j2\pi(f_p t + \frac{B}{T}\cdot\frac{t^2}{2})}\,\mathrm{rect}_T(t)$$

- CHIRP MODULUS DEL |s(t)|:

$$|s(t)| = \begin{cases} 1 & \text{Per } |t| \le T/2 \\ 0 & \text{Per } |t| \ge T/2 \end{cases}$$

- CHIRP PHASE Φ(t)

$$\Phi(t) = 2\pi(f_p t + \frac{B}{T}\cdot\frac{t^2}{2})$$

- INSTANTANEOUS FREQUENCY f(t)

$$f(t) = \frac{1}{2\pi}\cdot\frac{d\Phi(t)}{dt} = f_p + \frac{B}{T}t$$

$$f(-T/2) = f_p - B/2$$

$$f(T/2) = f_p + B/2$$

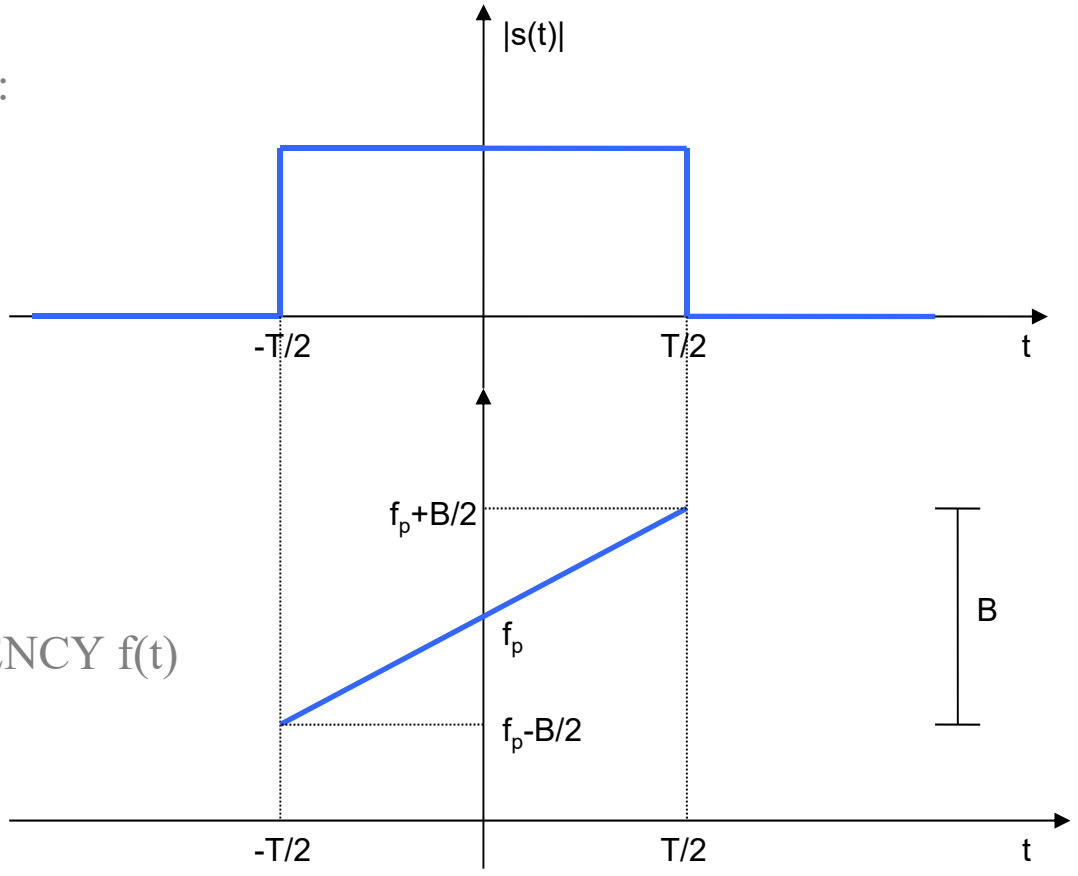

Frequency modulation

CHIRP: Time domain waveform (II)

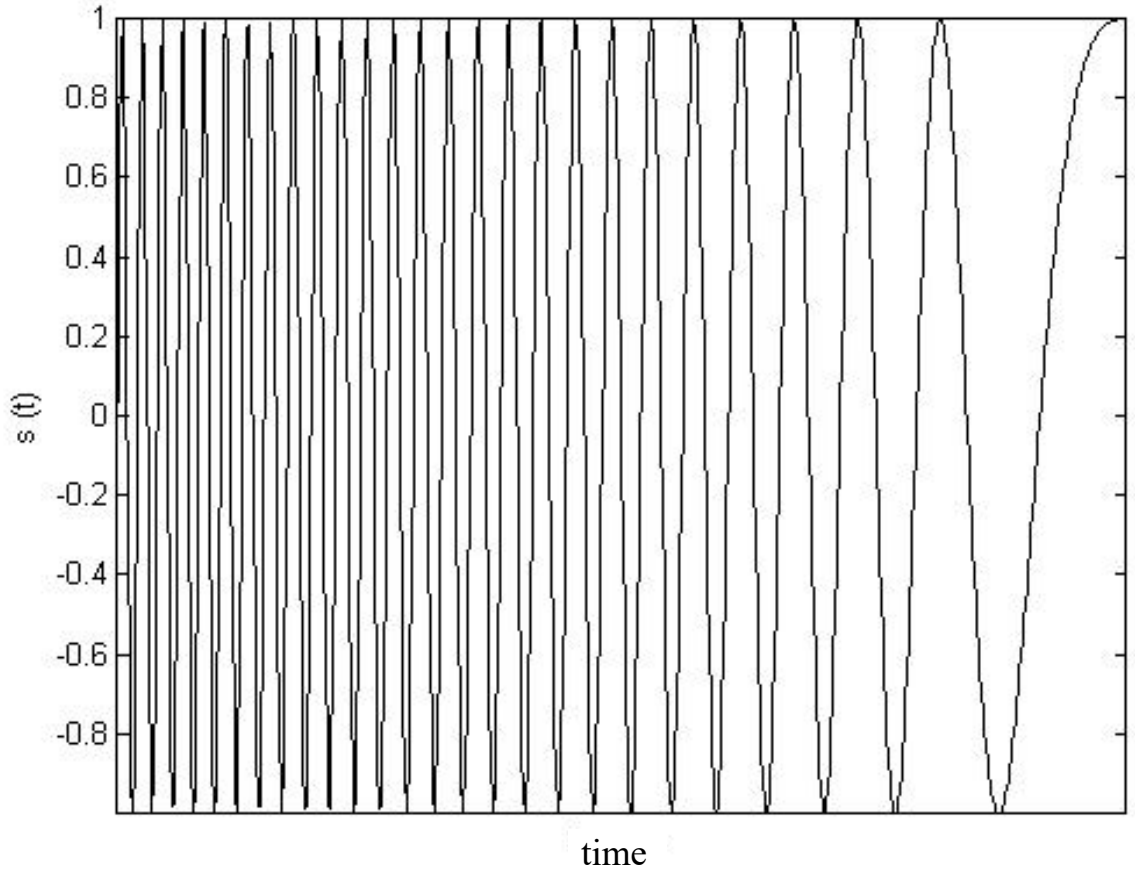

CHIRP: Time domain waveform (III)

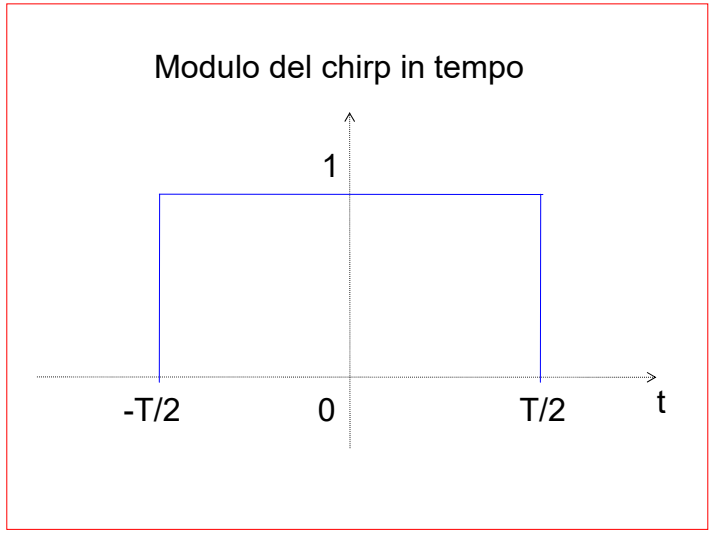

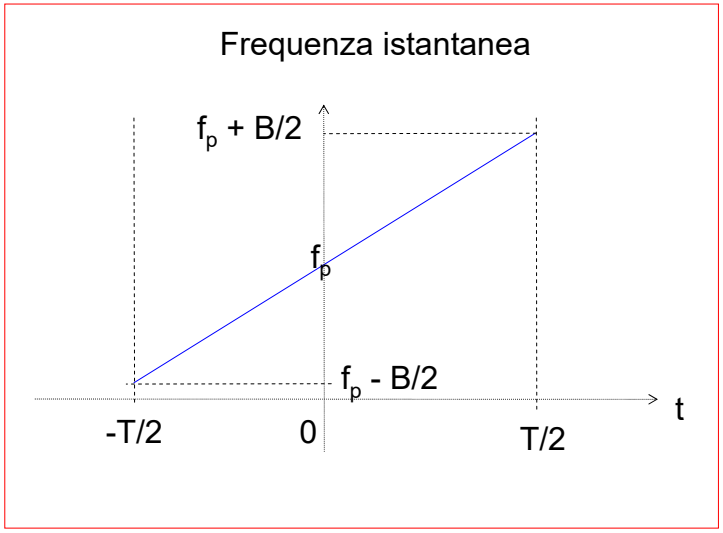

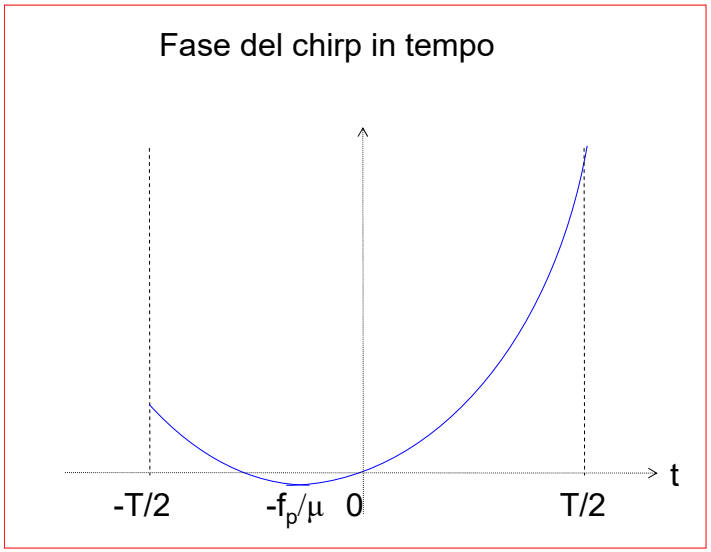

CHIRP: Frequency domain waveform (I)

Fourier Transform of the chirp signal:

$$S(f)=\frac{1}{\sqrt{2\mu}}\{[C(X_1)+C(X_2)]+j[S(X_1)+S(X_2)]\}e^{-j\frac{\pi}{\mu}f^2}=|S(f)|e^{j\Phi(f)}$$

C(X) Fresnel cosine
S(X) Fresnel sine

$$X_1=\sqrt{2BT}\left(\frac{1}{2}+\frac{f}{B}\right)$$

$$X_2=\sqrt{2BT}\left(\frac{1}{2}-\frac{f}{B}\right)$$

- ✓ The compression factor BT determines the frequency domain characteristics of the chirp waveform

AMPLITUDE SPECTRUM

$$|S(f)|=\frac{1}{\sqrt{2\mu}}\sqrt{[C(X_1)+C(X_2)]^2+[S(X_1)+S(X_2)]^2}$$

For high BT values (BT>100)

$$|S(f)|\cong\frac{1}{\sqrt{2\mu}}\sqrt{2}=\frac{1}{\sqrt{\mu}}=\sqrt{\frac{T}{B}} \qquad |f|\le B/2$$

PHASE SPECTRUM

$$\Phi(f)=-\frac{\pi}{\mu}f^2+\text{atg}\left[\frac{S(X_1)+S(X_2)}{C(X_1)+C(X_2)}\right]$$

For high BT values (BT>100)

$$\Phi(f)\cong-\frac{\pi}{\mu}f^2+\frac{\pi}{4} \qquad |f|\le B/2$$

$$S(f)=\sqrt{\frac{T}{B}}e^{-j\left[\pi\frac{T}{B}f^2-\frac{\pi}{4}\right]}\text{rect}_B(f)$$

Funzioni Coseno e Seno Integrale

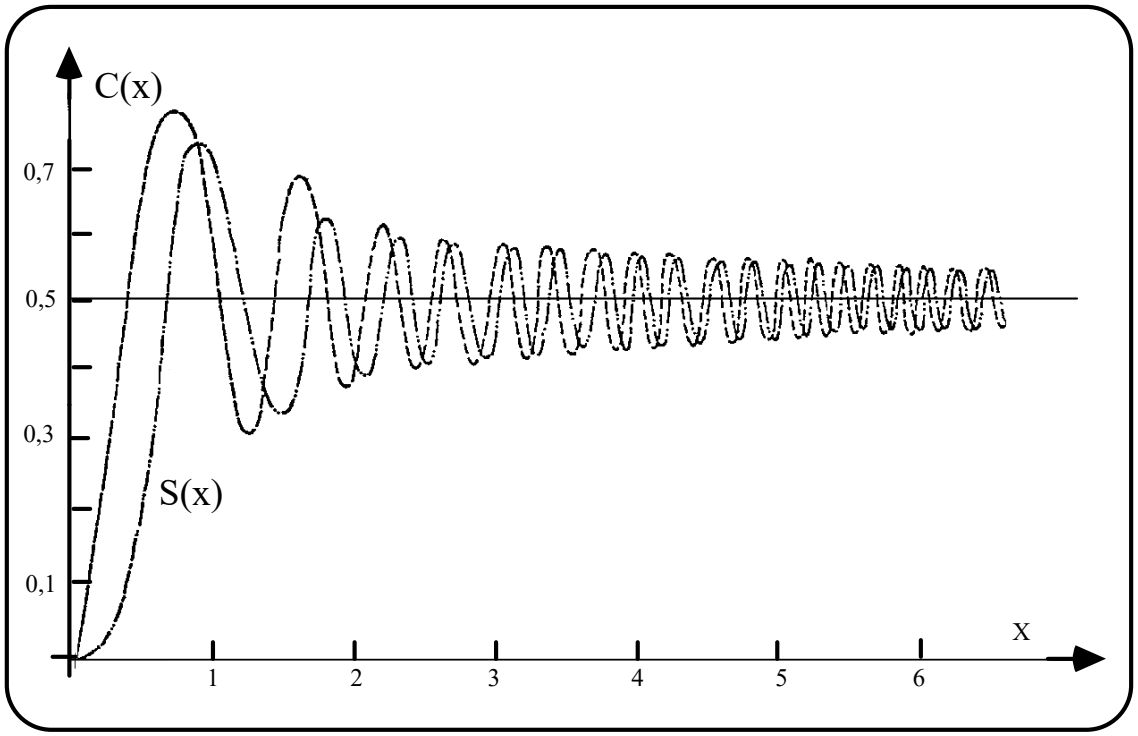

CHIRP: Frequency domain waveform (II)

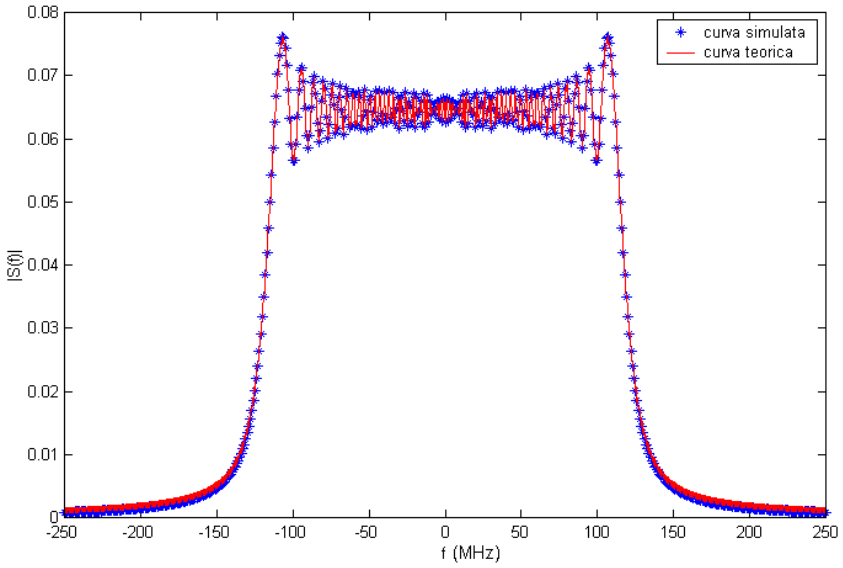

Chirp amplitude spectrum for B=240MHz, T=1μs

Chirp phase spectrum for B=240MHz, T=1μs

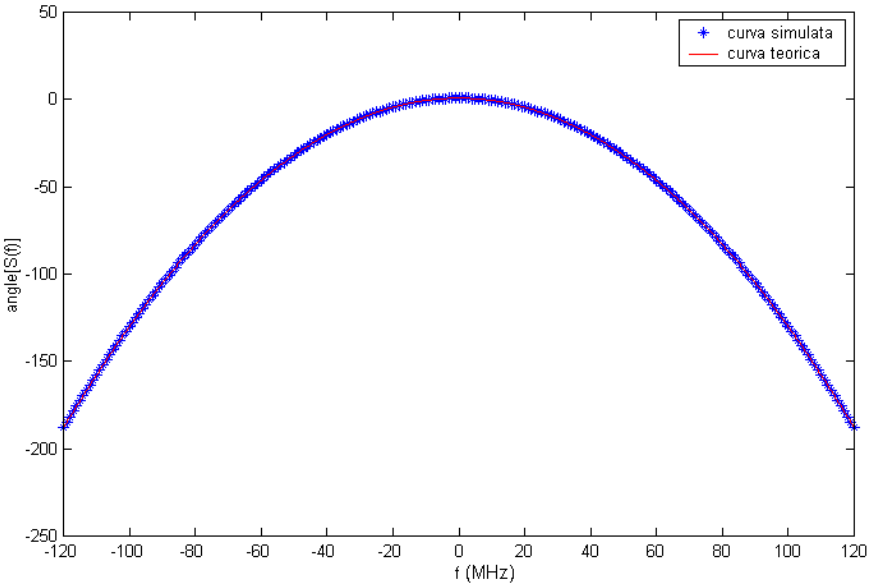

CHIRP: Frequency domain waveform (III)

Unmodulated RF pulse.
$t_p.\beta_3 = 1.$

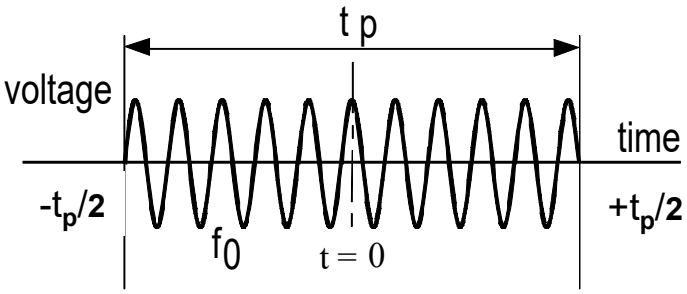

UP-sweep linear
FM chirp pulse.

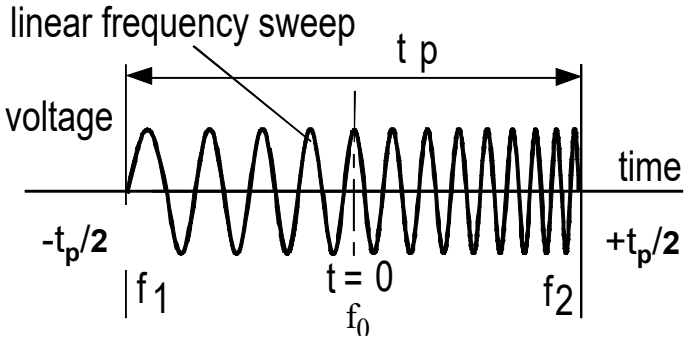

3dB bandwidth $\beta_3 = 1/ t_p$

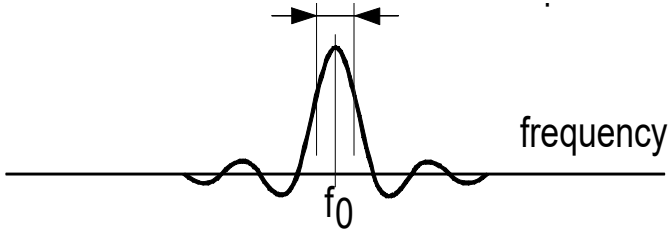

Sweep bandwidth $\beta_S = (f_2 - f_1)$

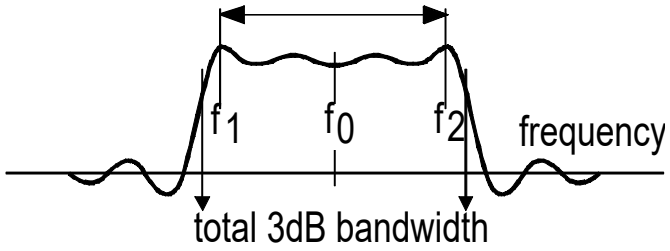

Autocorrelazione del chirp (I)

Funzione di Ambiguità: Chirp con inviluppo rettangolare

$$s_0(t) = \frac{1}{\sqrt{\tau_p}} rect_{\tau_p}(t)\, e^{j\pi k t^2}$$

$$|\chi(\tau,0)| = \left| (1-\frac{|\tau|}{\tau_p}) \sin c[\pi k \tau \tau_p (1-\frac{|\tau|}{\tau_p})] \right|, \qquad |\tau| \le \tau_p$$

Primo nullo

$$\pi k \tau \tau_p (1-\frac{|\tau|}{\tau_p}) = \pi$$

$$\tau \tau_p - \tau^2 = \frac{1}{k}$$

$$\tau^2 - \tau \tau_p + \frac{1}{k} = 0$$

$$\tau = \frac{\tau_p}{2} - \sqrt{\frac{\tau_p^2}{4} - \frac{1}{k}} =$$

$$= \frac{\tau_p}{2} - \frac{\tau_p}{2}\sqrt{1-\frac{4}{k\tau_p^2}} =$$

$$\approx \frac{\tau_p}{2} - \frac{\tau_p}{2}\left(1-\frac{2}{k\tau_p^2}\right) = \frac{1}{k\tau_p} = \frac{1}{B_p}$$

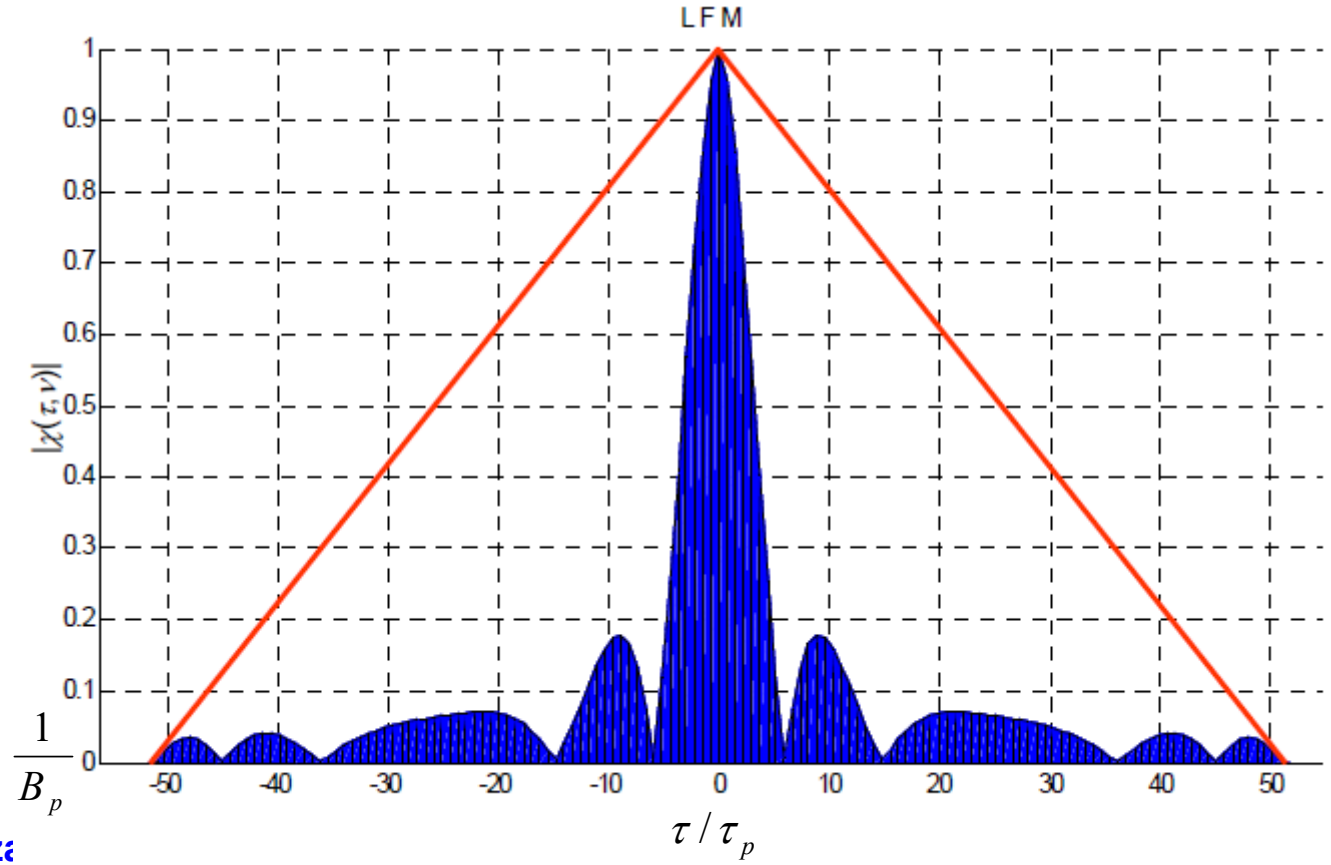

Funzione di autocorrelazione del chirp (III)

Funzione di Ambiguità: Chirp con inviluppo rettangolare

$$s_0(t) = \frac{1}{\sqrt{\tau_p}} rect_{\tau_p}(t)\ e^{j\pi k t^2}$$

$$\left|\chi(\tau,0)\right| = \left| (1-\frac{|\tau|}{\tau_p}) \sin c[\pi k \tau \tau_p (1-\frac{|\tau|}{\tau_p})] \right|, \qquad |\tau| \le \tau_p$$

Rapporto di compressione

$$\frac{\tau_p}{\frac{1}{k\tau_p}} = k\ \tau_p^2 = B_p\ \tau_p$$

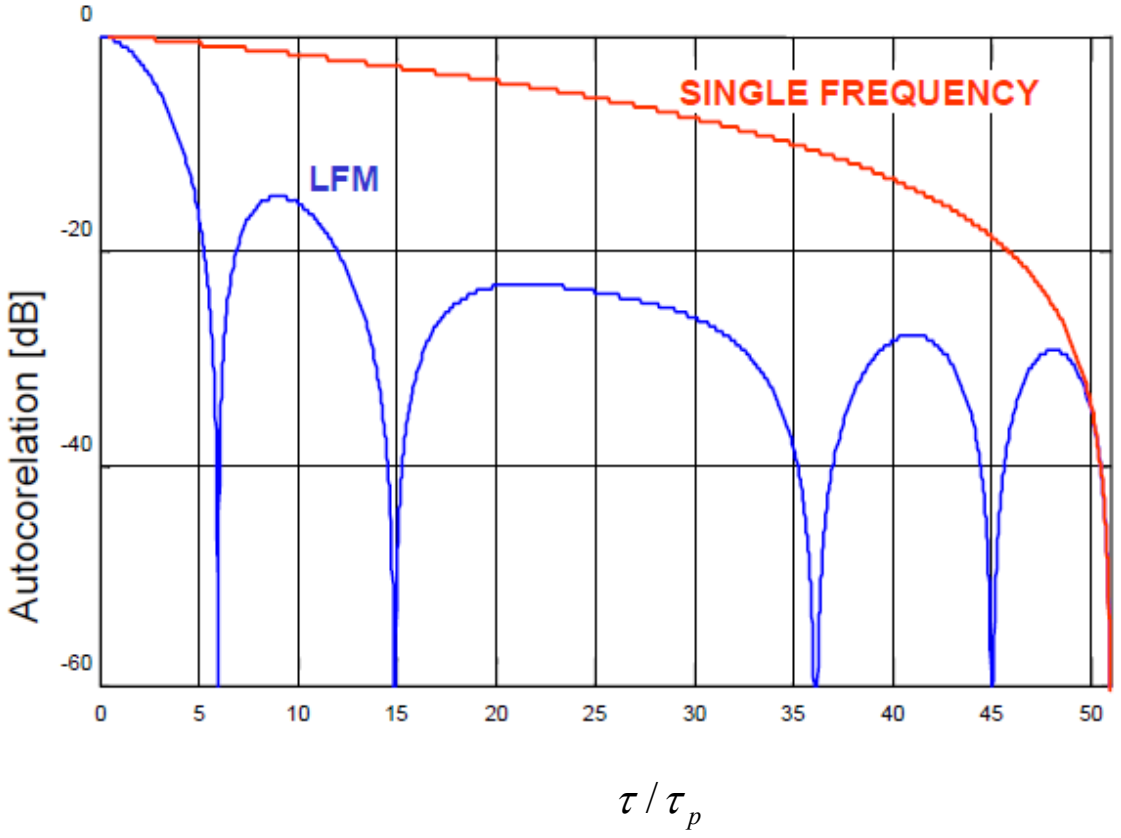

Chirp approximation and sidelobes (I)

- Chirp autocorrelation (matched filter output)

$$g(t) = \sqrt{\frac{B}{T}} \frac{\sin\left[\pi \frac{B}{T}\left(T - |t|\right)t\right]}{\pi \frac{B}{T} t}$$

- approximated with

$$g(t) \cong \sqrt{\frac{B}{T}} \frac{\sin[\pi B t]}{\pi \frac{B}{T} t} = \sqrt{BT}\ \sin c\ [\pi\, B\, t]$$

which is the Inverse Fourier Transform of a rectangle in the frequency domain

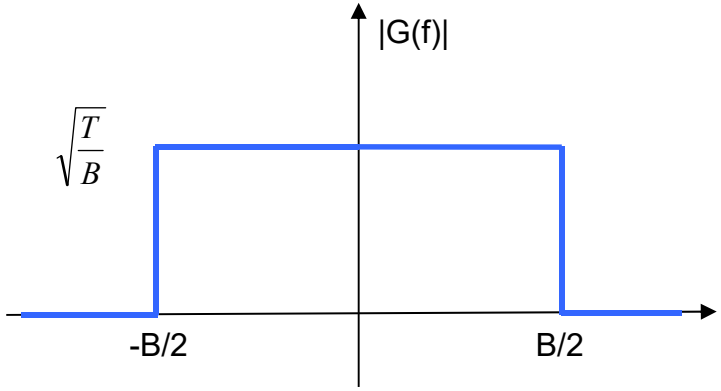

$$G(f) = \sqrt{\frac{T}{B}}\ rect_B(f)$$

Pulse compression technique (I)

- **Matched Filter**

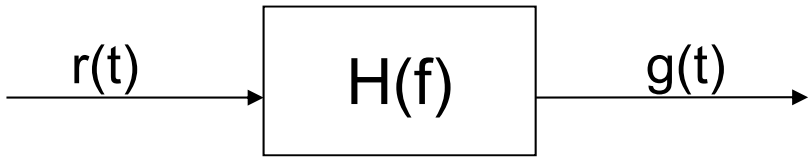

$$r(t) = e^{j2\pi\left(f_p t + \frac{B}{T}\cdot\frac{t^2}{2}\right)} \mathrm{rect}_T(t)$$ Received signal

$$h(t) = \sqrt{\frac{B}{T}} e^{-j2\pi\left(-f_p t + \frac{B}{T}\cdot\frac{t^2}{2}\right)} \mathrm{rect}_T(t)$$ matched filter impulse response

$$g(t) = r(t) * h(t) = \int_{-\infty}^{\infty} r(\tau) h(t-\tau) d\tau$$ matched filter output

$$g(t) = \sqrt{\frac{B}{T}} \frac{\mathrm{sen}\left[\pi \frac{B}{T}\left(T - |t|\right)t\right]}{\pi \frac{B}{T} t} \cdot e^{j2\pi f_p t}$$

sin x/x signal envelope:
with -4dB aperture =1/B.

✓ g(t) autocorrelation of the input signal (f_d=0).
✓ for $f_d \neq 0$ mismatched filter

The pulse has been compressed to:
$\tau_c = 1/B < T$

Pulse compression technique (II)

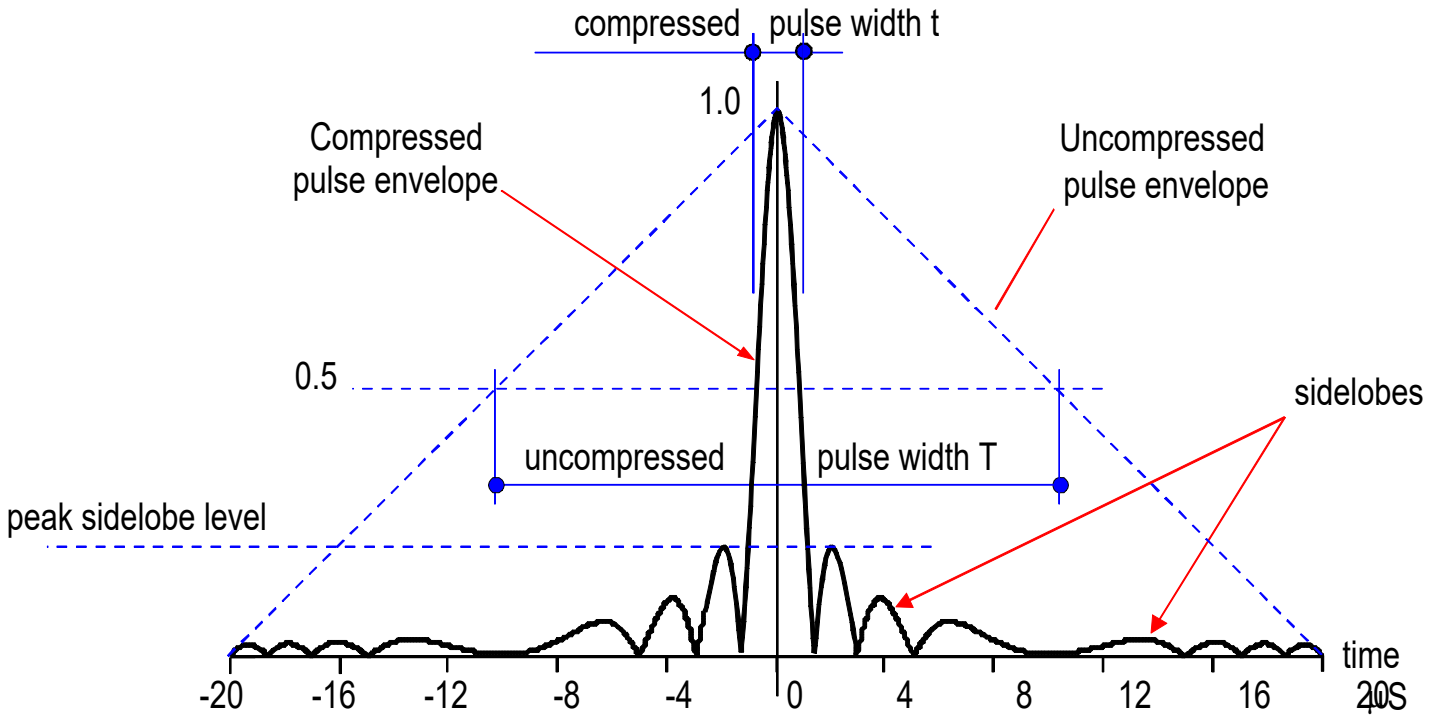

The width of the main lobe of the compressed pulse is $1/\beta_s$ ie. $\frac{1}{\text{sweep bandwidth}}$

Pulse compression technique (III)

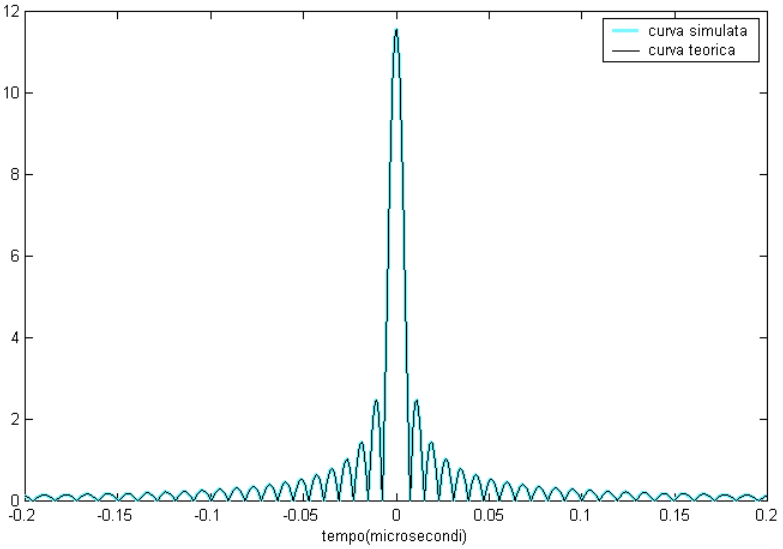

Matched filter output

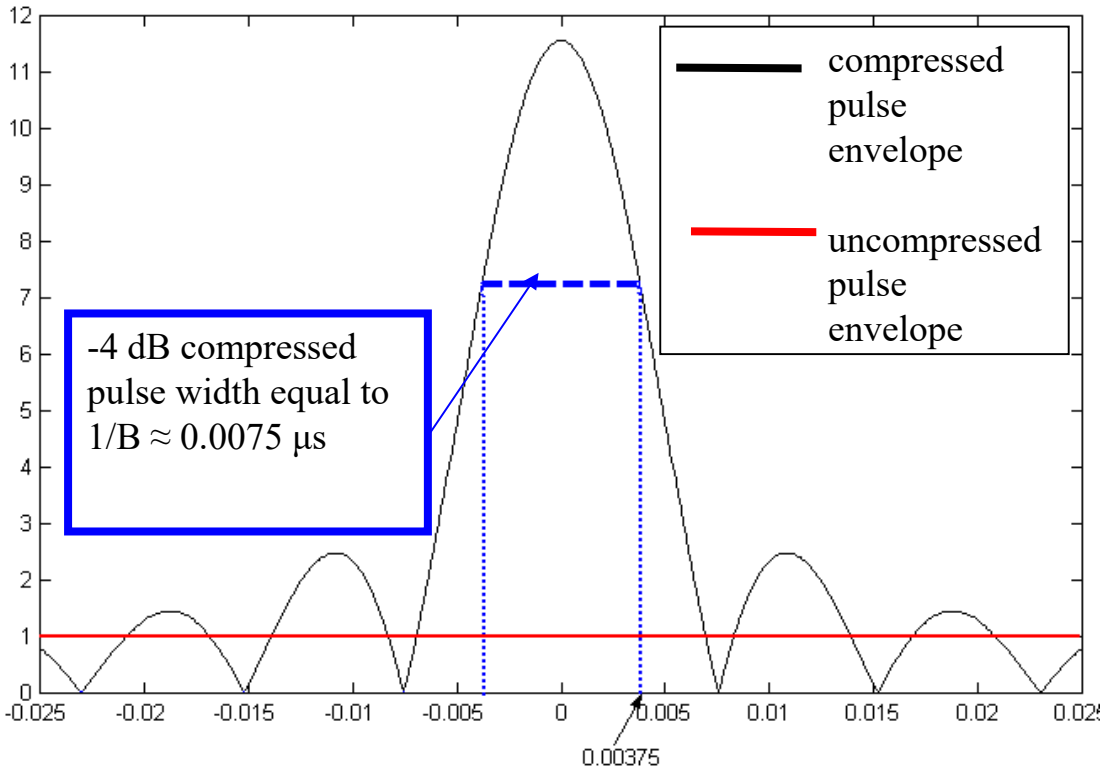

Matched filter output for: B=133.5 MHz and T=1 μs

Pulse compression technique (IV)

Matched filter output : sidelobes

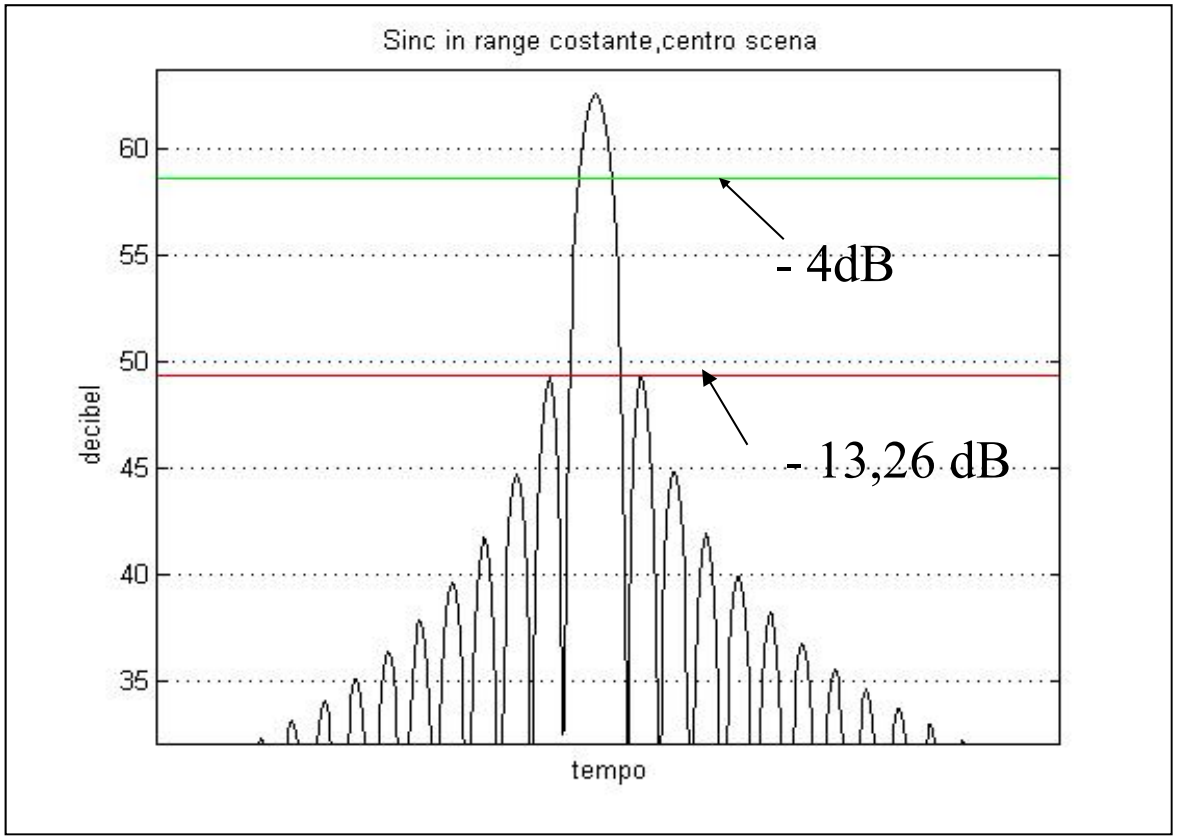

SAW pulse compression (I)

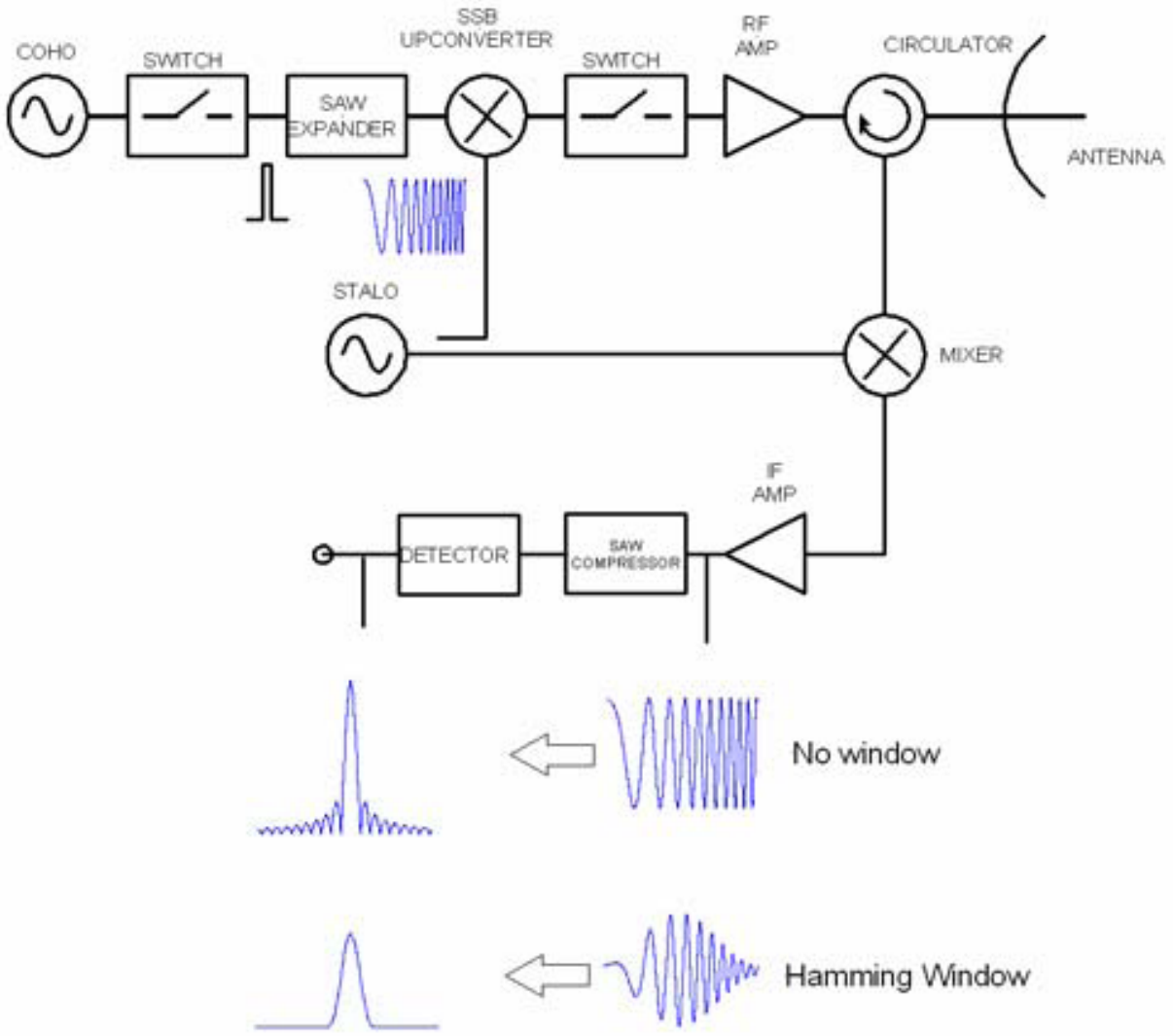

Radiotecnica e

SAW pulse compression (II)

- In a pulse compression system, a very brief pulse consisting of a range of frequencies passes through a dispersive delay line (SAW expander) in which its components are delayed in proportion to their frequency.
- In the process the pulse is stretched; for example a 1ns pulse may be lengthened by a factor of 1000 to a duration of 1μs before it is up-converted amplified and transmitted.
- A constant amplitude waveform is produced in which the frequency increases or decreases linearly by Δf over the duration of the pulse

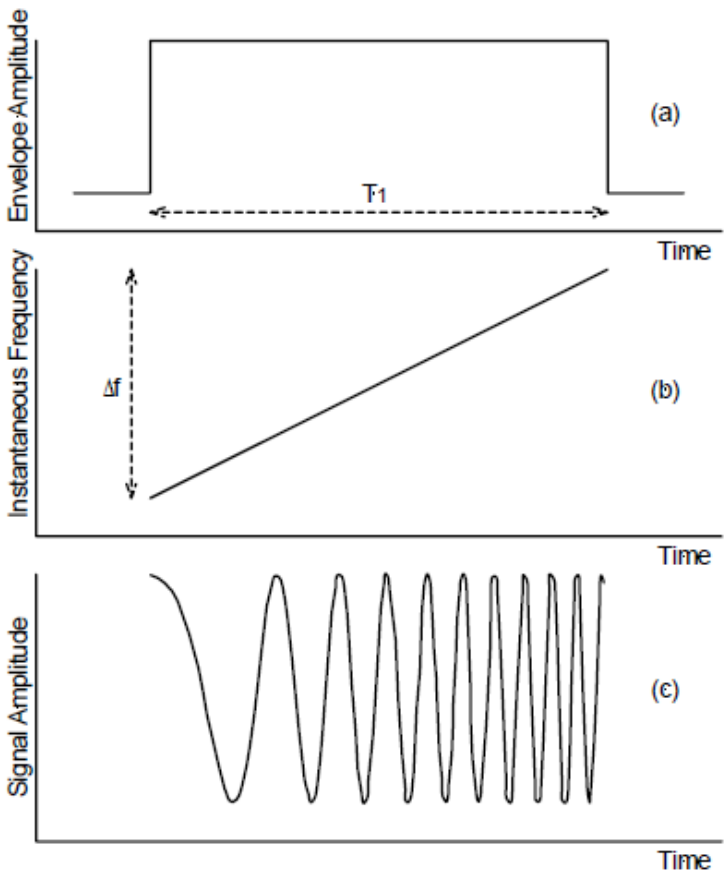

SAW pulse compression (III)

- The echo returns from the target are down converted and amplified
- It is then passed through a pulse compression filter which is designed so that the velocity of propagation is proportional to frequency
- The pulse is compressed to a width $1/\Delta f$
- The compressed echo yields nearly all of the information that would have been available had the unaltered 1ns pulse been transmitted.
- The amount of signal-to-noise ratio (SNR) gain achieved is approximately equivalent to the pulse time-bandwidth product $\beta.\tau$.
- Most pulse compression systems use surface acoustic wave (SAW) technology to implement the pulse expansion and compression functions
- The maximum $\beta.\tau$ product that is readily available is about 1000.

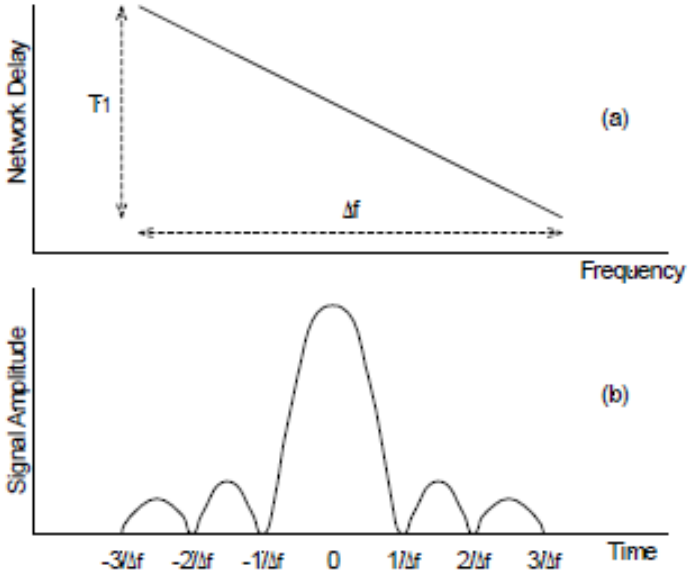

SAW pulse compression (IV)

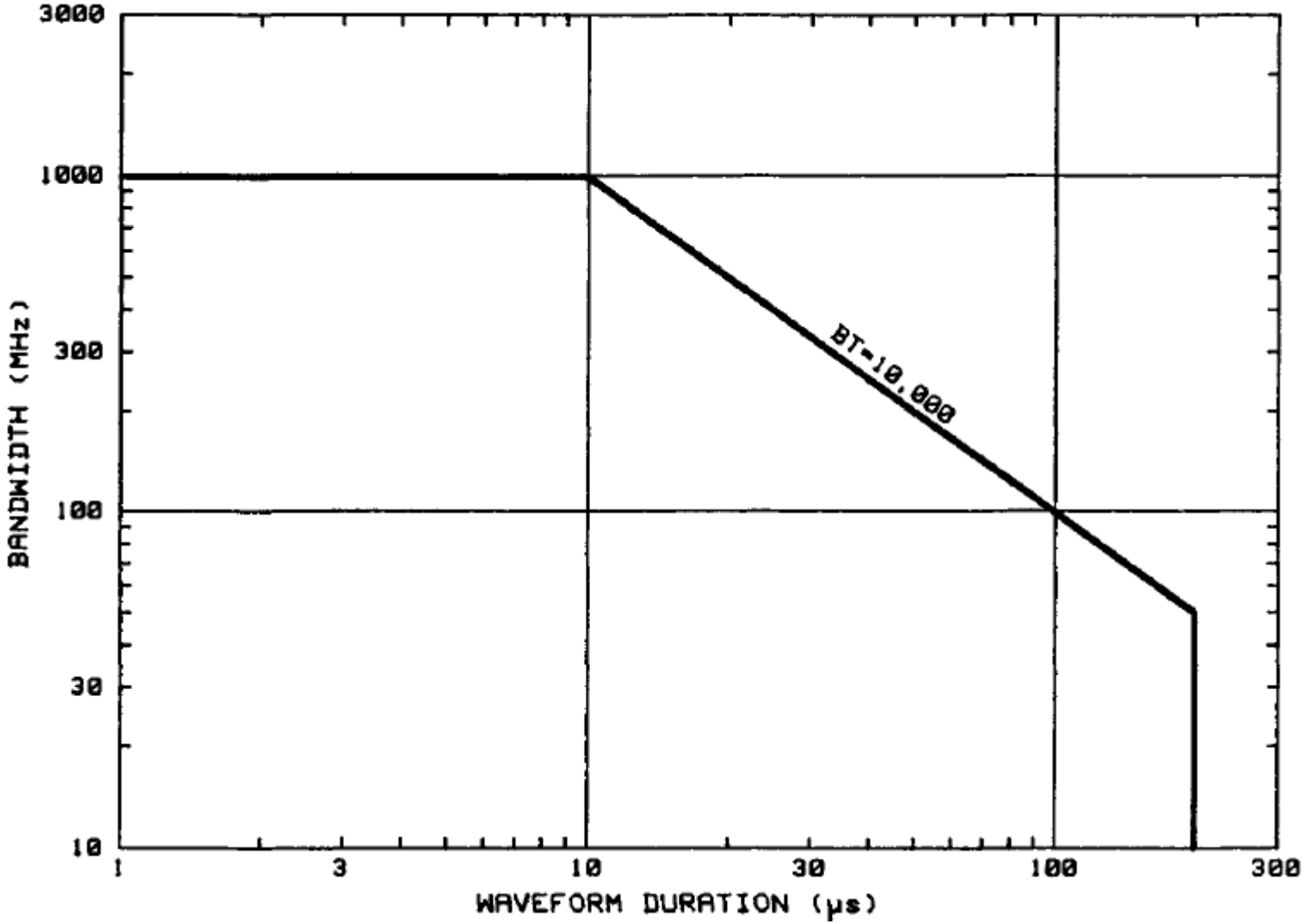

Chirp approximation and sidelobes

- Chirp autocorrelation (matched filter output)

$$g(t) = \sqrt{\frac{B}{T}} \frac{\sin\left[\pi \frac{B}{T}\left(T - |t|\right)t\right]}{\pi \frac{B}{T} t}$$

- approximated with

$$g(t) \cong \sqrt{\frac{B}{T}} \frac{\sin[\pi B t]}{\pi \frac{B}{T} t} = \sqrt{BT}\ \sin c\ [\pi\, B\, t]$$

which is the Inverse Fourier Transform of a rectangle in the frequency domain

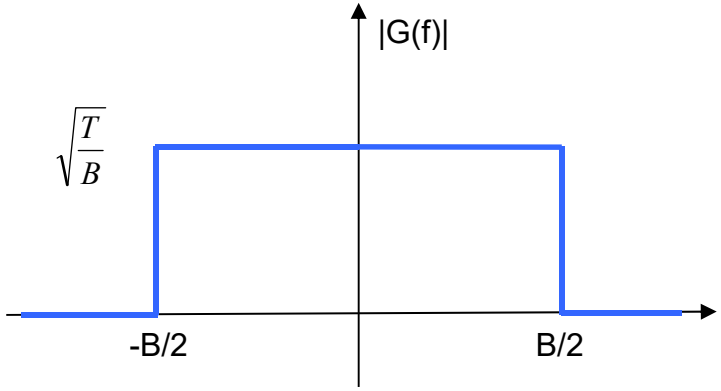

$$G(f) = \sqrt{\frac{T}{B}}\ rect_B(f)$$

Distorsioni lineari (I)

Effetto delle distorsioni

- Il sistema reale sarà affetto da distorsioni (non sarà esattamente uguale a quello ideale): tutte le distorsioni di sistema possono essere sintetizzate in un filtro distorcente posto in cascata al filtro adattato ideale:

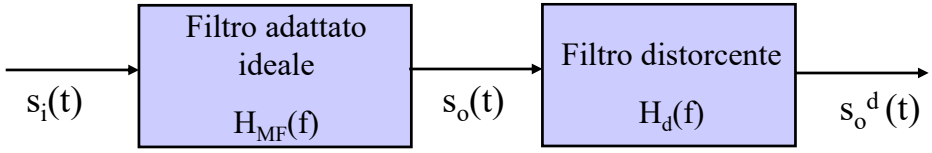

- Nell'ipotesi di piccole distorsioni la $H_d(f)$ può essere sviluppata in serie arrestandosi al primo termine

$$H_d(f) = A(f)e^{jB(f)} \rightarrow \begin{cases} A(f) = 1 + a_1 \cos(2\pi C_a f) \\ e^{jB(f)} = e^{jb_1 \sin(2\pi C_b f)} \cong 1 + jb_1 \sin(2\pi C_b f) \end{cases}$$

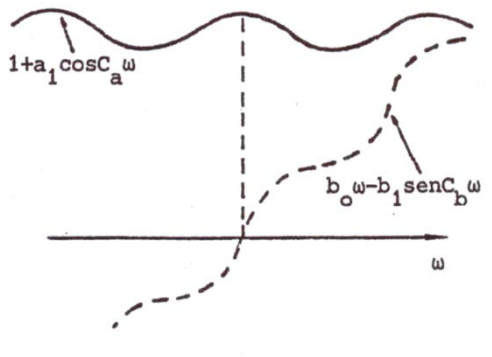

a_1: valore di picco della componente di ampiezza;
b_1: valore di picco della componente di fase;
C_a: frequenza ripple di ampiezza;
C_b: frequenza ripple di fase;

Distorsioni lineari (II)

- Il segnale di uscita distorto è dato da:

$$s_o^d(t) = s_o(t) + \frac{a_1}{2} s_o(t + C_a) + \frac{a_1}{2} s_o(t - C_a) \longrightarrow \text{effetto della distorsione di ampiezza;}$$

$$s_o^d(t) = s_o(t) + \underbrace{\frac{b_1}{2} s_o(t + C_b) - \frac{b_1}{2} s_o(t - C_b)}_{\textbf{ECHI APPAIATI}} \longrightarrow \text{effetto della distorsione di fase;}$$

L'utilizzo di filtri reali anziché ideali comporta la presenza di un disturbo additivo dato dagli echi appaiati: tanto maggiore è a_1&b_1 tanto maggiore è l'ampiezza dell'eco, tanto minore è C_a&C_b (ripple lento) tanto più gli echi appaiati compaiono vicini al segnale utile $\Rightarrow$ dalle specifiche di dinamica si può ricavare la massima distorsione ammissibile (valore massimo a_1&b_1).

Frequency domain weighting (I)

- To control sidelobes of the compressed waveform, amplitude weighting with appropriate tape functions can be used

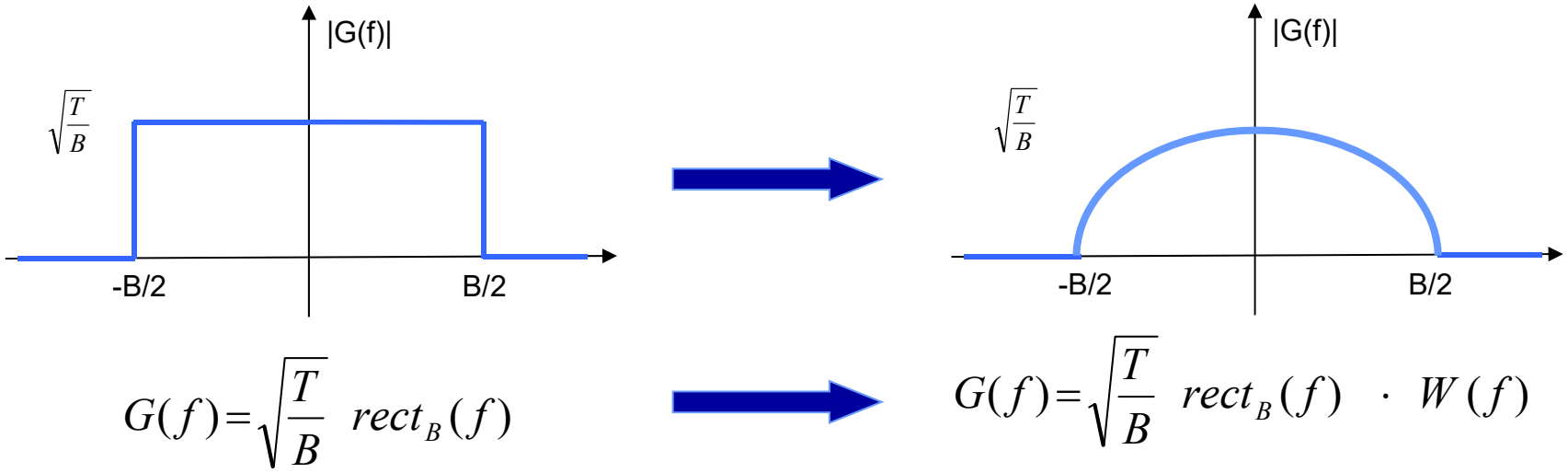

$$G(f) = \sqrt{\frac{T}{B}}\ rect_B(f) \qquad G(f) = \sqrt{\frac{T}{B}}\ rect_B(f)\ \cdot\ W(f)$$

Taking the Inverse Fourier Transform, we have in time domain

$$g(t) \cong \sqrt{BT}\ \ \text{sinc}\ [\pi\, B\, t] \qquad g(t) \cong \sqrt{BT}\ \ \text{sinc}\ [\pi\, B\, t] * \ w(t)$$

Frequency domain weighting (II)

- using appropriate taper function, allows to control sidelobes

For example

$$W(f) = (1-k) + k\ \cos(\pi \frac{f}{B})$$

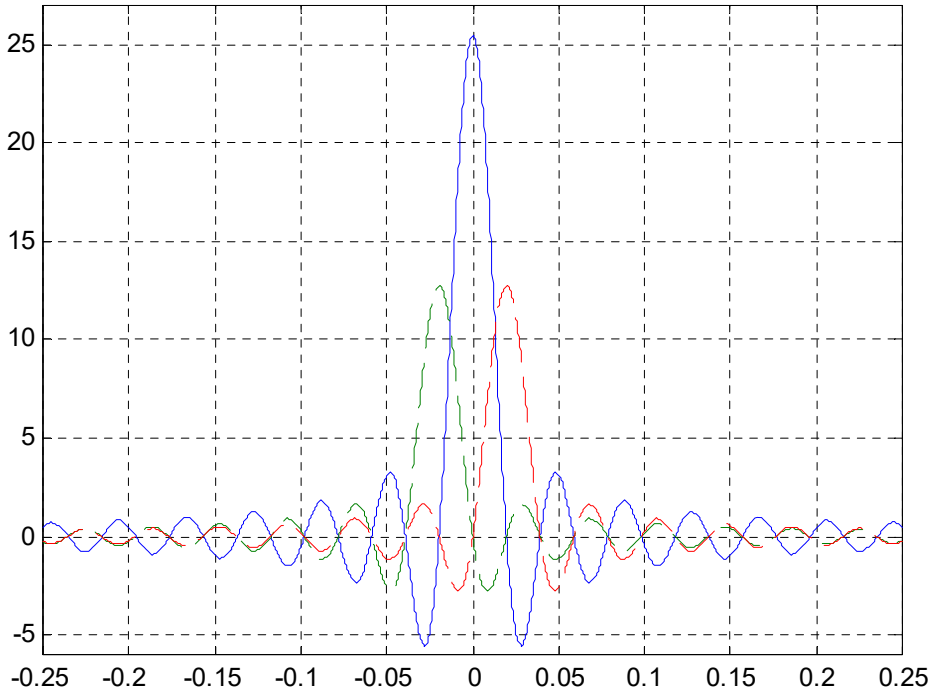

$$w(t) = (1-k)\ \delta(t) + \frac{k}{2}\ \delta(t - \frac{1}{2B}) + \frac{k}{2}\ \delta(t + \frac{1}{2B})$$

Shifted replicas to remove sidelobes …

$$g(t) \cong \sqrt{BT}\ \left\{ (1-k)\ \text{sinc}\ [\pi\, B\, t] + \frac{k}{2}\ \text{sinc}\ \left[\pi\, B\, (t - \frac{1}{2B})\right] + \frac{k}{2}\ \text{sinc}\ \left[\pi\, B\, (t - \frac{1}{2B})\right] \right\}$$

Analog vs. Digital domain operations

- usually compression is applied in the sampled domain
- Starting from an approximately rectangular chirp spectrum (sampled in frequency at 1/T)

$$g(t_n) = \sum_{k=-\frac{(N-1)}{2}}^{\frac{(N-1)}{2}} e^{+j\frac{2\pi}{T}k t_n} = \frac{\sin\left[\frac{\pi}{T}(N-1)t_n\right]}{\sin\left[\frac{\pi}{T}t_n\right]}$$

Zeros of NUM: $t_n = \frac{kT}{N-1}$

Zeros of DEN: $t_n = kT$

which is the Inverse Fourier Transform of a rectangle in the frequency domain

$$g(t_n) = \sum_{k=-\frac{(N-1)}{2}}^{\frac{(N-1)}{2}} w_k\, e^{+j\frac{2\pi}{T}k t_n} \qquad \text{with} \qquad w_k = W(\frac{k}{T})$$

Compressed waveform quality parameters

- **Side Lobe Level**

$$SLL = \frac{\text{Amplitude of the highest Side Lobe}}{\text{Main Beam Peak}}$$

  Side Lobe Ratio

$$SLR = (SLL)^{-1}$$

$w_k \rightarrow$ taper coefficients

↕ Generally achieved at the expense of:

- **Efficiency**

$$\eta = \frac{\left(\sum_{k=0}^{N-1} w_k\right)^2}{N\sum_{k=0}^{N-1} w_k^2}$$

- **3 dB resolution**

Taylor (1953):

- Symmetric weights yield lower sidelobes
- The sidelobe decay depends on the discontinuity in the aperture distribution and in its derivatives.
- A weight distribution with non-zero external elements (pedestal) is more efficient

Common used taper functions

	Efficiency η	PSL (dB)	Main lobe width (w.r.t) 1/B.
Uniform	1	-13.3	0.89
Cosine	0.81	-23	1.19
Cosine squared (Hanning)	0.67	-32	1.44
Cosine squared on 10 dB pedestal	0.88	-26	1.08
Cosine squared on 20 dB pedestal	0.75	-40	1.28
Hamming	0.73	-43	1.30
Dolph Chebyshev	0.72	-50	1.33
Dolph Chebyshev	0.66	-60	1.44
Taylor n-bar=3	0.9	-26	1.05
Taylor n-bar=5	0.8	-36	1.18
Taylor n-bar=8	0.73	-46	1.30

Triangle (Bartlett) Window

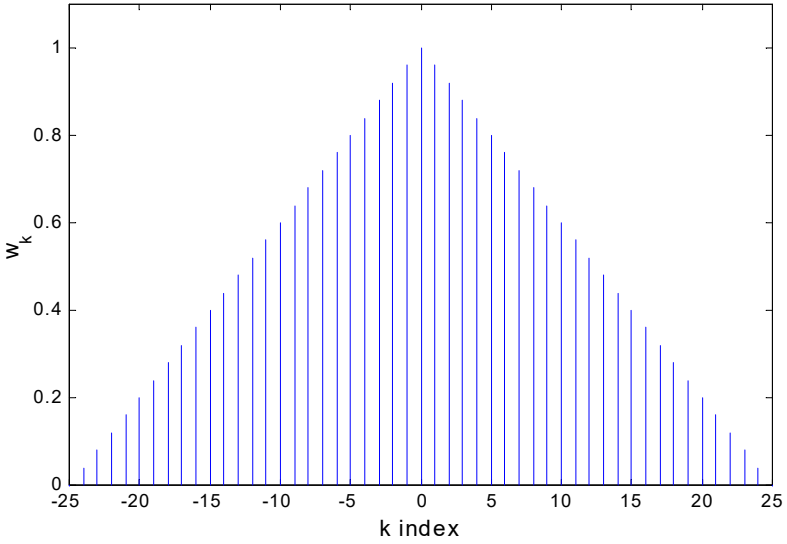

$$w_k = 1 - \frac{|k|}{(N-1)/2} \qquad k = -\frac{N-1}{2},..,-1,0,1,..,\frac{N-1}{2}$$

$$g(t_n) = \frac{2}{N}\left[\frac{\sin\left[\frac{\pi}{T}\frac{N}{2}t_n\right]}{\sin\left[\frac{\pi}{T}t_n\right]}\right]^2$$

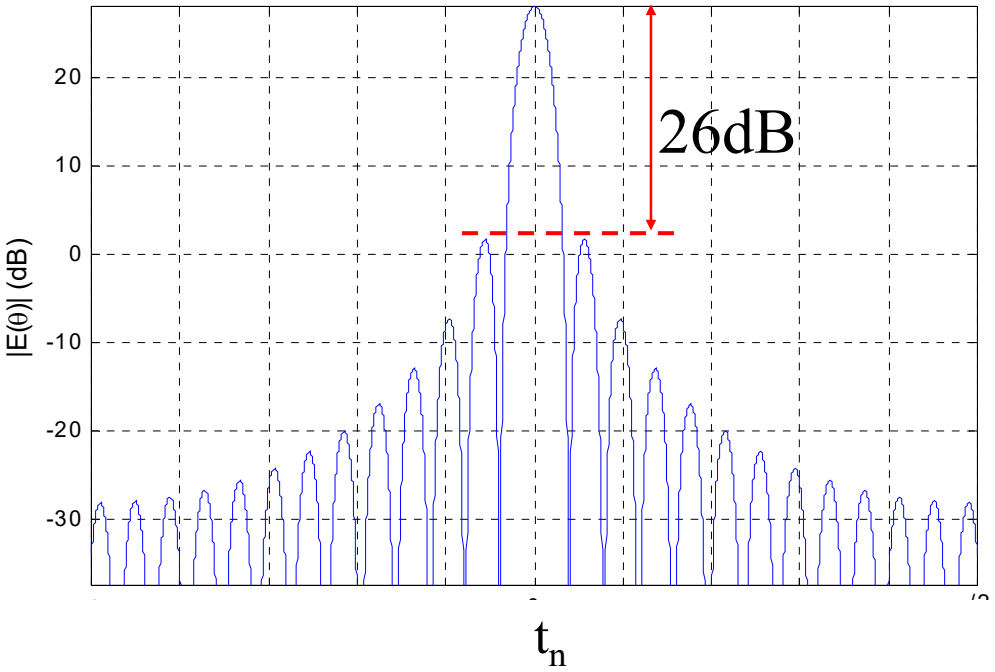

- Main Beam width (between zero crossing) is twice that of the uniform window
- Zeros of order 2 in the Fourier Transform
- SLR≅26dB=2*13dB
- Decay SL ∝ $1/x^2$ (-12dB/oct) (discontinuity in the first derivative)

$\cos^{\alpha}(x)$ Windows

$$w_k = \cos^{\alpha}\left[\frac{k}{N-1}\pi\right] \qquad k = -\frac{N-1}{2},..,-1,0,1,..,\frac{N-1}{2}$$

As α increases, the windows become smoother and the pattern shows increased SLR and faster falloff of the SL, but with an increase width of the ML.

α=1

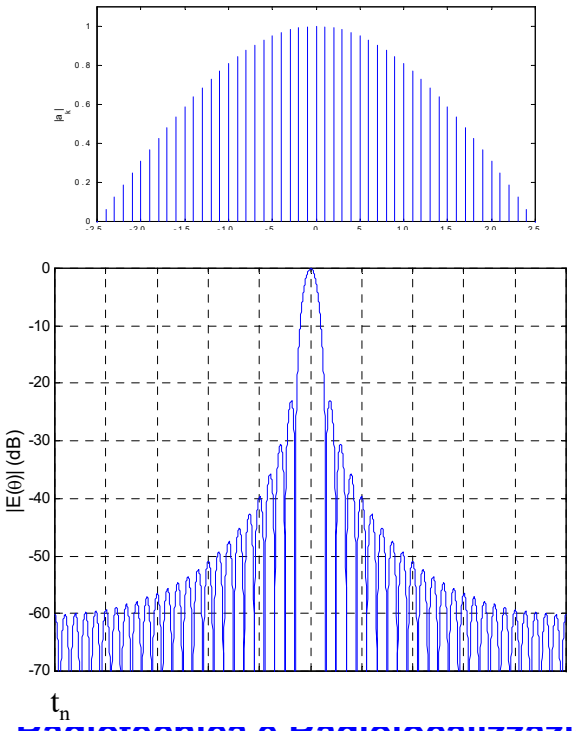

α=2

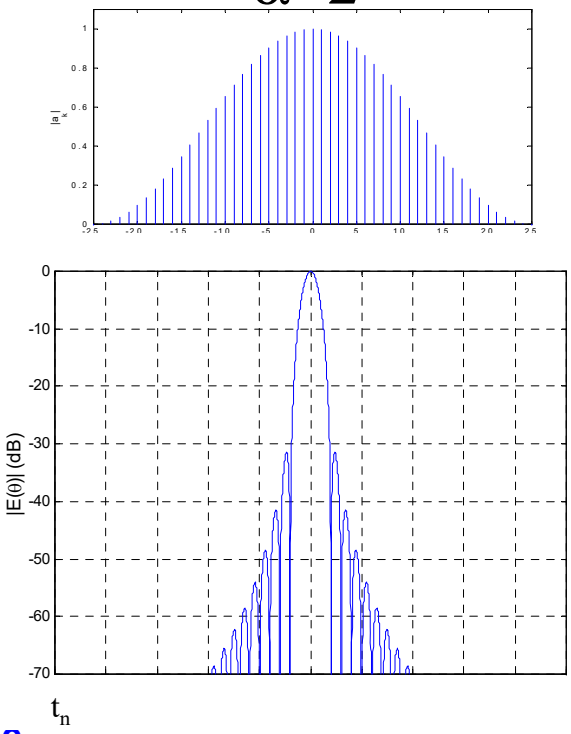

α=3

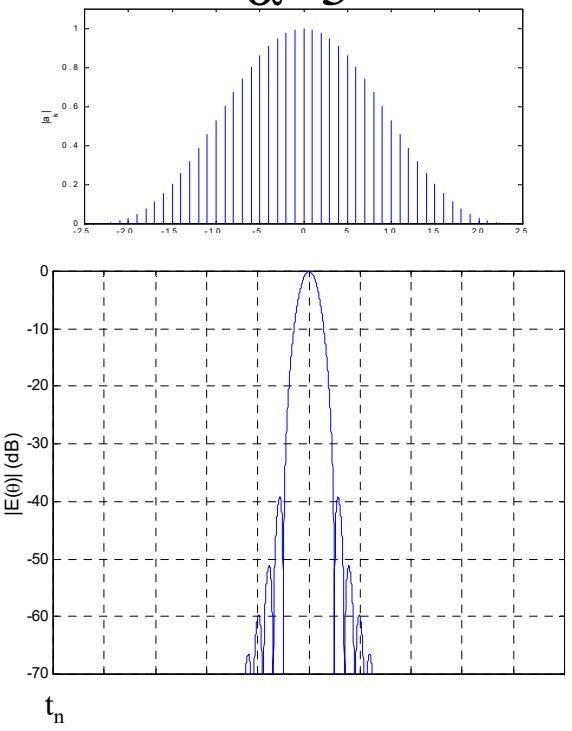

$\cos^{\alpha}(x)$ Windows → Hanning Window ($\alpha=2$)

$$w_k = \cos^2\left[\frac{k}{N-1}\pi\right] = \frac{1}{2}\left[1+\cos\left[\frac{2k}{N-1}\pi\right]\right] = \frac{1}{2}+\frac{1}{2}\cos\left[\frac{2k}{N-1}\pi\right] \qquad k = -\frac{N-1}{2},..,-1,0,1,..,\frac{N-1}{2}$$

$$g(t_n) = \left\{\frac{1}{2}D(x)+\frac{1}{4}\left[D\left(x+\frac{\pi}{N}\right)+D\left(x-\frac{\pi}{N}\right)\right]\right\}$$

$$\left(D(x) = \frac{\sin\left[\frac{\pi}{T}N\,t_n\right]}{\sin\left[\frac{\pi}{T}t_n\right]}\right)$$

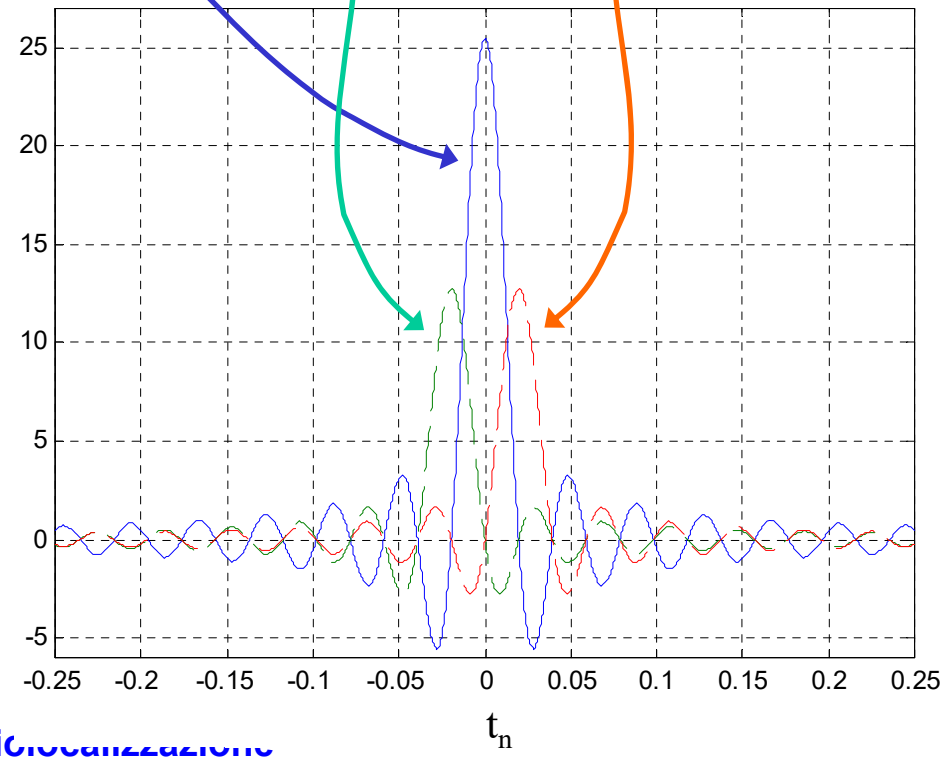

$\cos^{\alpha}(x)$ Windows → Hanning Window (α=2)

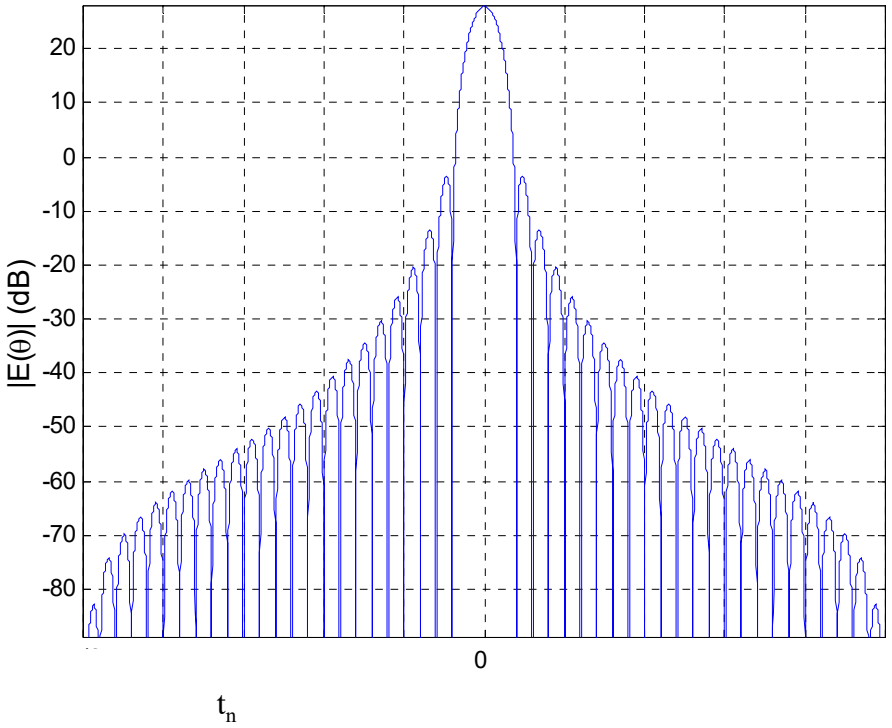

- It does not require extra memory and is controlled by a single parameter.
- Wide enlargement of the main lobe
- Low efficiency: η=0.67
- SLR=32dB
- SL Decay $\propto 1/x^3$ (-18dB/oct) (discontinuity in the second derivative)

Hamming Window (1/2)

The Hamming weights are a modified version of the Hanning weights:

$$\text{Hamming} \begin{cases} w_k = \frac{1}{2} + \frac{1}{2}\cos\left[\frac{2k}{N-1}\pi\right] & k = -\frac{N-1}{2},..,-1,0,1,..,\frac{N-1}{2} \\ g(t_n) = \left\{\frac{1}{2}D(x) + \frac{1}{4}\left[D\left(x+\frac{\pi}{N}\right) + D\left(x-\frac{\pi}{N}\right)\right]\right\} \end{cases}$$

It is obtained by modifying the coefficients of the combination of D(x) functions to achieve a better SL cancellation

$$\begin{cases} w_k = \gamma + (1-\gamma)\cos\left[\frac{2k}{N-1}\pi\right] & k = -\frac{N-1}{2},..,-1,0,1,..,\frac{N-1}{2} \\ g(t_n) = \left\{\gamma D(x) + \frac{1}{2}(1-\gamma)\left[D\left(x+\frac{\pi}{N}\right) + D\left(x-\frac{\pi}{N}\right)\right]\right\} \end{cases}$$

Cancellation of the first sidelobe is for γ=0.543478261. in practice, it is used γ=0.54:

$$\text{Hamming} \begin{cases} w_k = 0.54 + 0.46\cos\left[\frac{2k}{N-1}\pi\right] & k = -\frac{N-1}{2},..,-1,0,1,..,\frac{N-1}{2} \\ g(t_n) = \left\{0.54D(x) + \frac{1}{2}0.46\left[D\left(x+\frac{\pi}{N}\right) + D\left(x-\frac{\pi}{N}\right)\right]\right\} \end{cases}$$

Hamming Window (2/2)

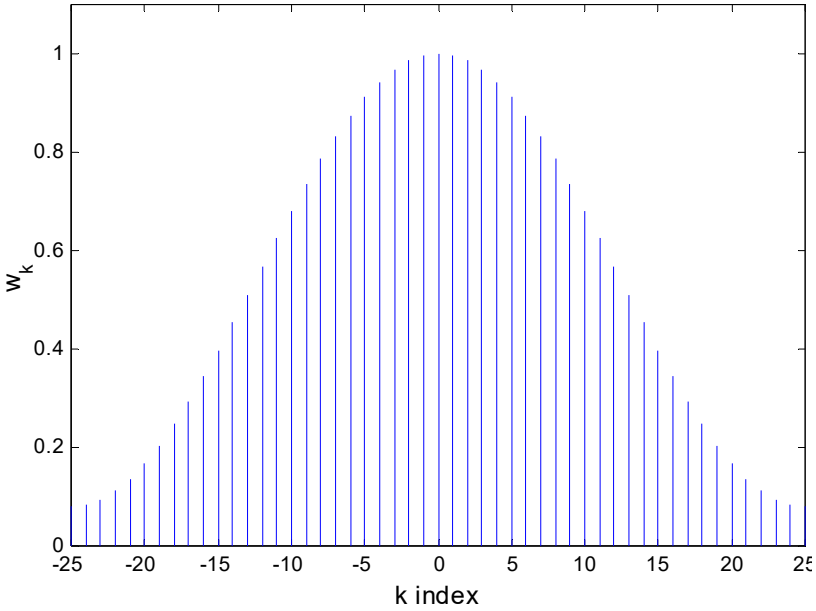

- SLR=43dB
- SL Decay $\propto$ 1/x (-6dB/oct) (discontinuity at the extremes)

- large attenuation of the first SL of the original compressed waveform
- Better efficiency than Hanning: η=0.73

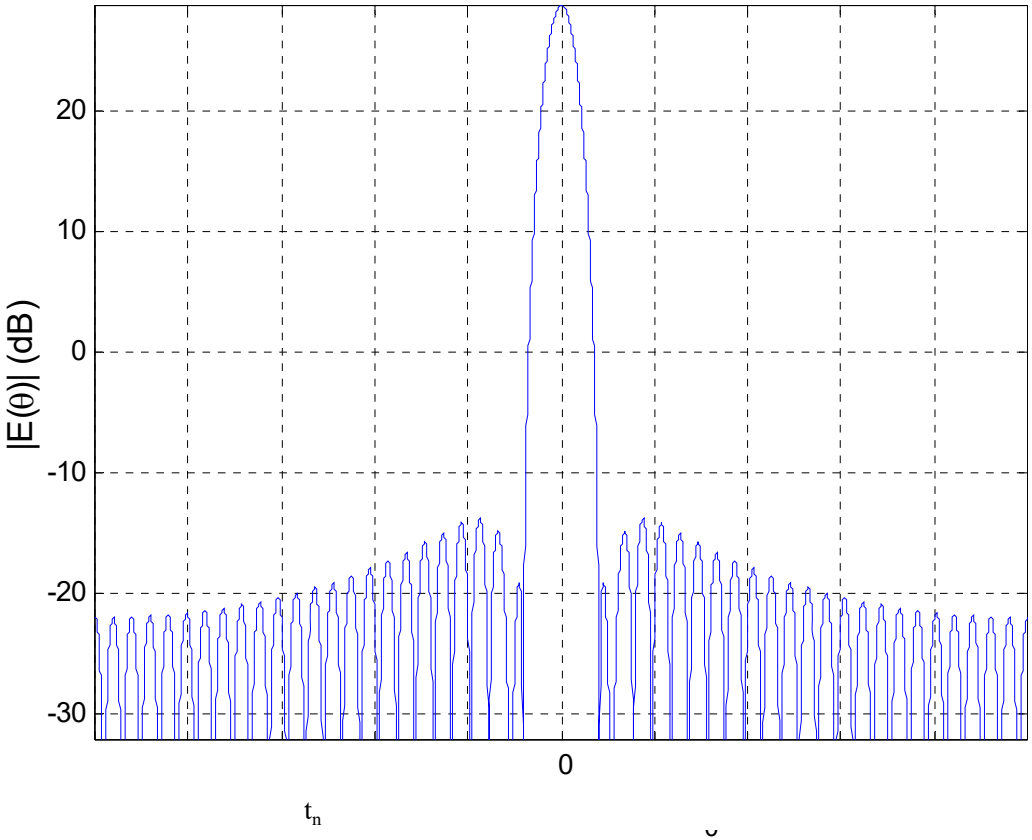

Blackman Windows

- Hanning and Hamming taper functions belong to the "raised cosine" family
- Both are special cases of the Blackman windows (windows function of (N+1)/2 parameters) with only γ_0 and γ_1 non-zero coefficients :

$$w_k = \sum_{m=0}^{(N-1)/2} \gamma_m \cos\left(\frac{2\pi}{N-1} mk\right) \qquad \sum_{m=0}^{(N-1)/2} \gamma_m = 1 \qquad k = -\frac{N-1}{2},..,-1,0,1,..,\frac{N-1}{2}$$

Difficulties with the family of windows:

- The choice of parameters to achieve the desired waveform characteristics is difficult (complex inversion)
- Often the characteristics are not adequate in terms of resolution and efficiency.

Dolph-Chebyshev Window (1/3)

It provides the maximal resolution for assigned sidelobe (costant) level!

The design is based on the properties of the **Chebyshev polynomials** :

$$T_n(u)=\begin{cases}(-1)^n \cosh(n\cosh^{-1}|u|) & u<-1\\ \cos(n\cos^{-1}u) & |u|\le 1\\ \cosh(n\cosh^{-1}u) & u>1\end{cases}$$

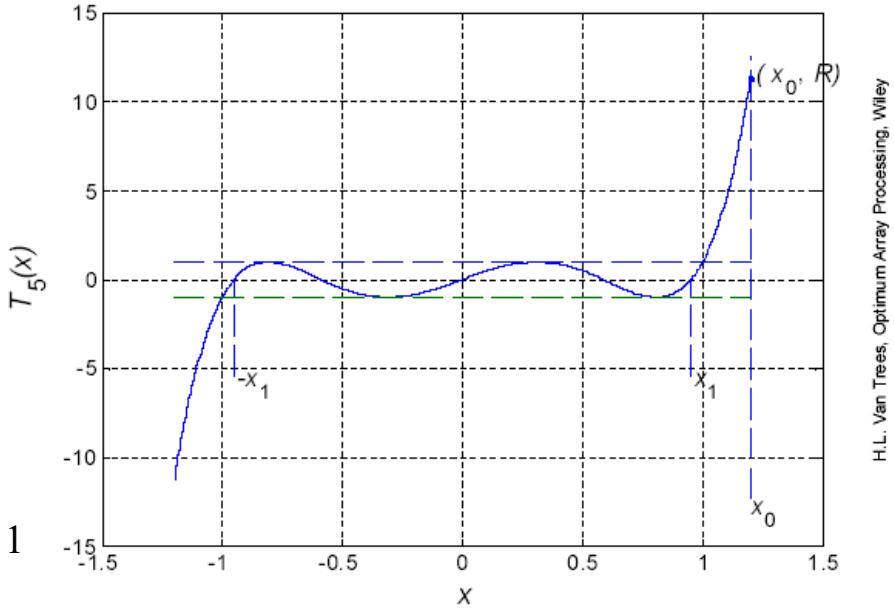

Properties:

- $T_n(u)=2uT_{n-1}(u)-T_{n-2}(u)$
- Zeros in $|u|\le 1, u_p = \cos\left[(2p-1)\frac{\pi}{2n}\right] \quad p=1,..,n$
- Maxima and minima in $u_k = \cos\left[\frac{k\pi}{n}\right] \quad k=1,..,n-1$
- Also $T_n(u_k) = \pm 1$

For a window of N elements, a polynomial with order n=N-1 is used (N-1 zeros).
The oscillating part of the polynomial is used for the sidelobes, while the main lobe is mapped in the region x>1.

Dolph-Chebyshev Window (2/3)

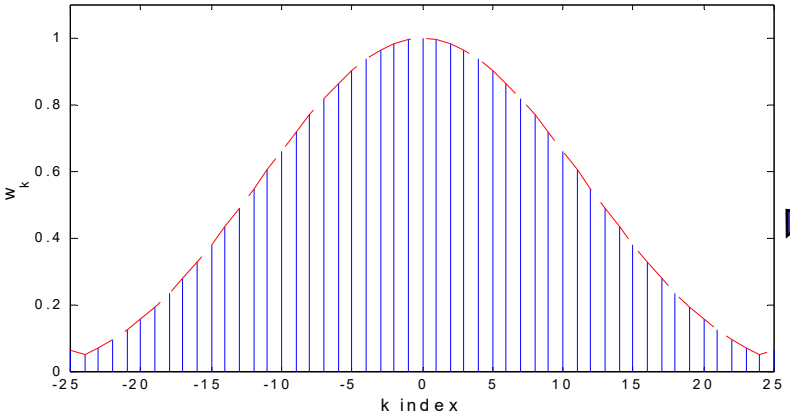

SLR=50dB

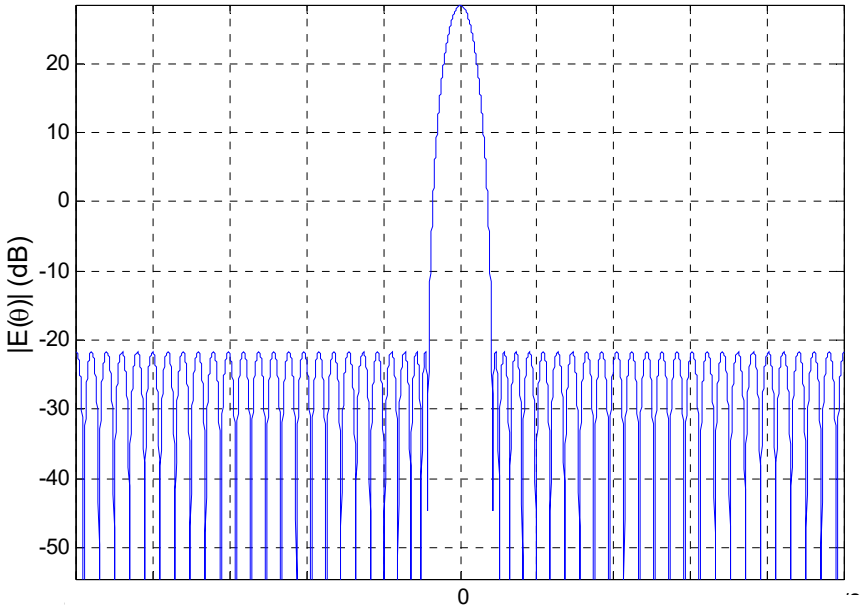

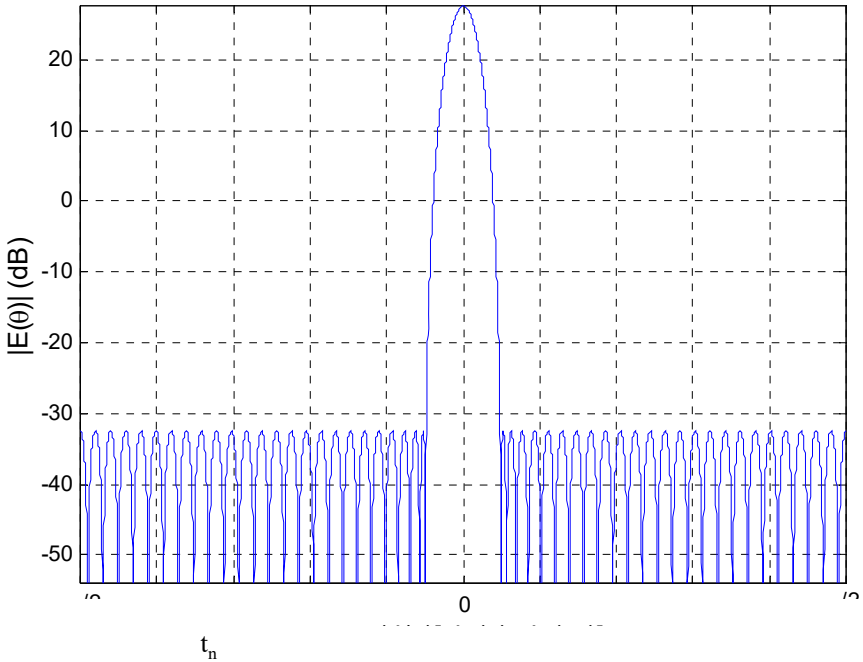

SLR=60dB

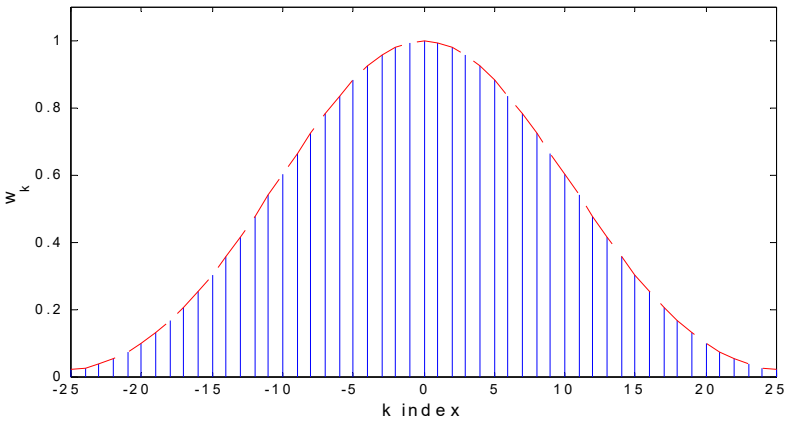

Dolph-Chebyshev Window (3/3)

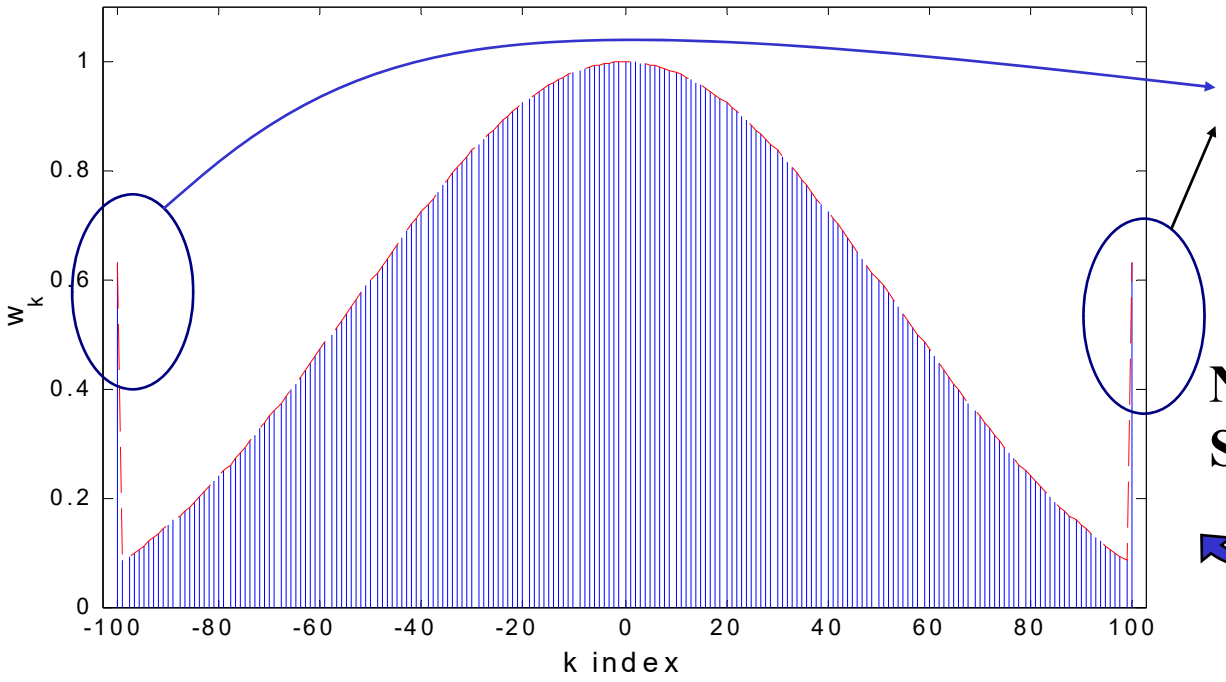

Spike in the taper function!!

N=201
SLR=40dB

For this reason, such taper function is not used in practice.
The Taylor taper function is studied to solve such undesired feature, while keeping the nice properties of the Dolph-Chebyshev solution.

Taylor n-bar Window (1/4)

This is a trade-off between Dolph-Chebyshev taper function with constant RSL and the uniform weights with 1/x sidelobe decay.

Starting point

$$\begin{cases} F(u)=\cosh\left[\pi\sqrt{A^2-u^2}\right] & u\le A \\ F(u)=\cos\left[\pi\sqrt{u^2-A^2}\right] & u\ge A \end{cases}$$

- $u=2x/\pi$
- Pattern with constant level sidelobes
- There is a transition in the main lobe at u=A between the hyperbolic function and the trigonometric function
- Zeros at → $z_n=\pm\sqrt{A^2+(n-1/2)^2}$
- SLR=F(0)=$(1/\pi)\cosh A$

Strategy

Using this ideal pattern, there are still spikes at the window borders → an approximate pattern is used where:

- The first $\bar{n}$ sidelobes are maintained at a constant level
- The pattern zeros are moved to achieve a 1/u behavior in the sidelobe level region far from the main beam

Taylor n-bar Window (2/4)

New zeros:

$$\begin{cases} z_n = \pm\sigma\sqrt{A^2 + (n-1/2)^2} & 1 \le n \le \bar{n} \\ z_n = \pm n & n \ge \bar{n} \end{cases}$$

$$\sigma = \frac{\bar{n}}{\sqrt{A^2 + (\bar{n} - 1/2)^2}}$$

$$F(u) = \frac{\sin \pi u}{\pi u} \prod_{n=1}^{\bar{n}-1} \frac{1 - \left(\frac{u}{z_n}\right)^2}{1 - \left(\frac{u}{n}\right)^2}$$

Inversion

$$w_k = \left[1 + 2 \sum_{n=1}^{\bar{n}-1} F(n, A, \bar{n}) \cos\left(n\pi \frac{2k}{(N-1)}\right) \right] / w_{MAX}$$

with $$F(n, A, \bar{n}) = \frac{[(\bar{n}-1)!]^2}{(\bar{n}-1+n)!(\bar{n}-1-n)!} \prod_{m=1}^{\bar{n}-1} \left[1 - \left(\frac{n}{z_m}\right)^2 \right]$$

$$k = -\frac{N-1}{2}, .., -1, 0, 1, .., \frac{N-1}{2}$$

Taylor n-bar Window (3/4)

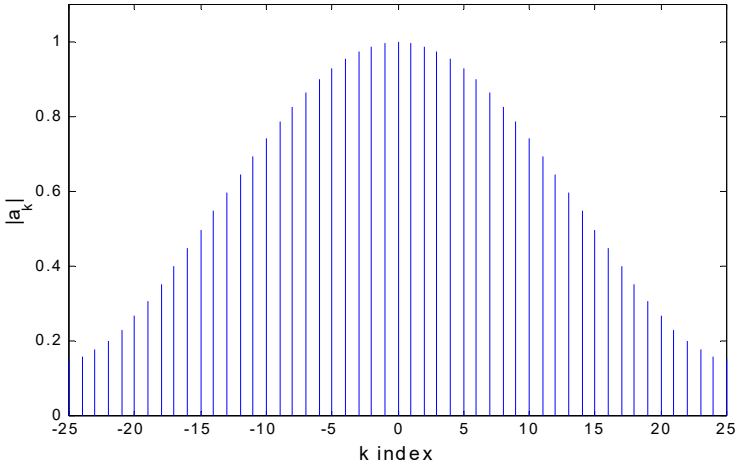

$\bar{n}=5$

SLR=36dB

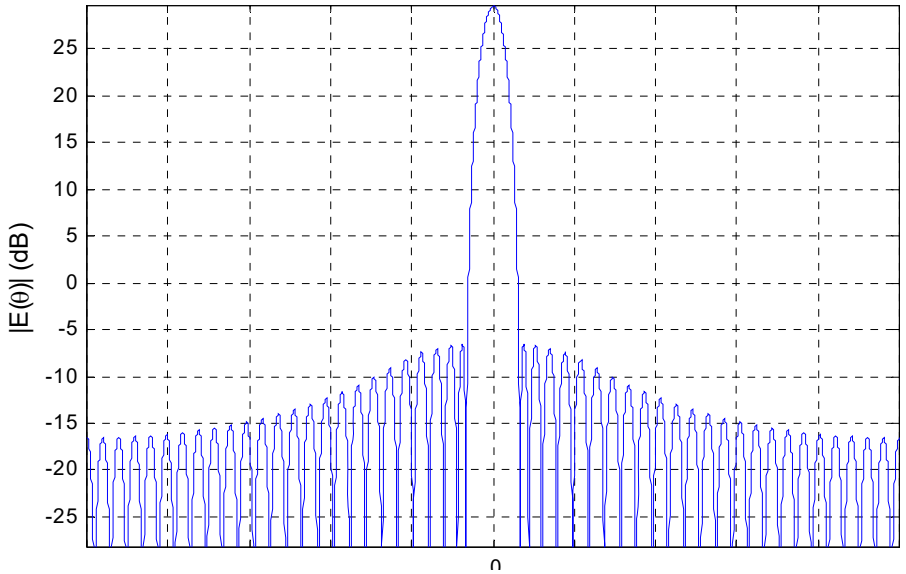

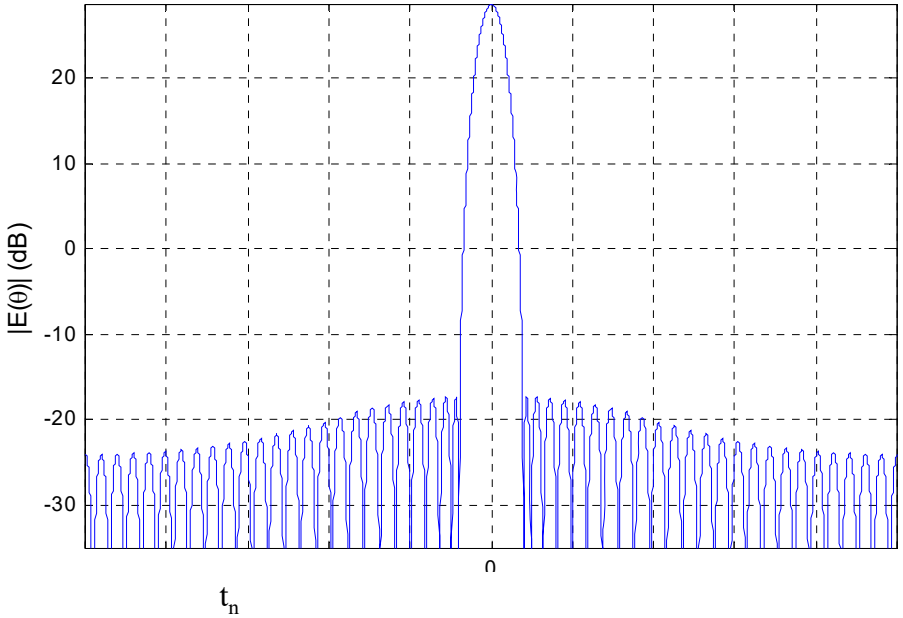

$\bar{n}=8$

SLR=46dB

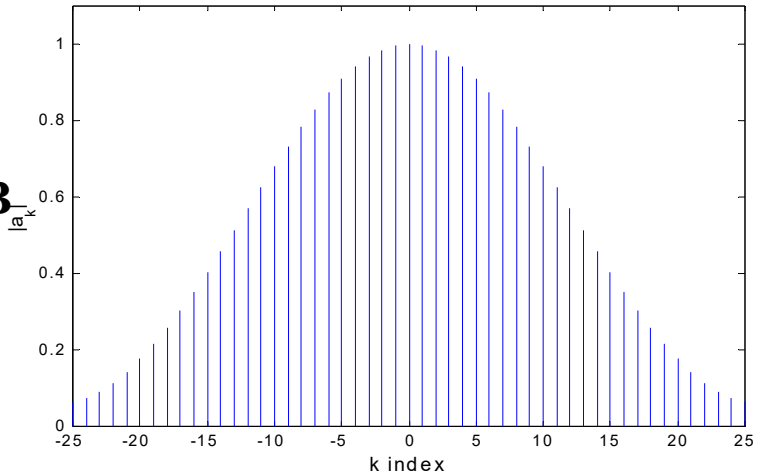

Taylor n-bar Window (4/4)

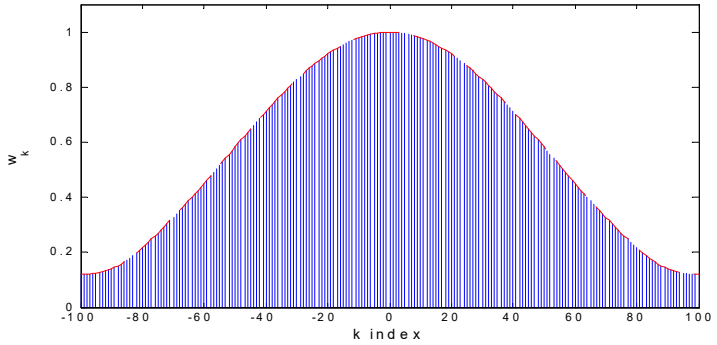

$\bar{n}$ =10
N=201
SLR=40dB

No spikes!

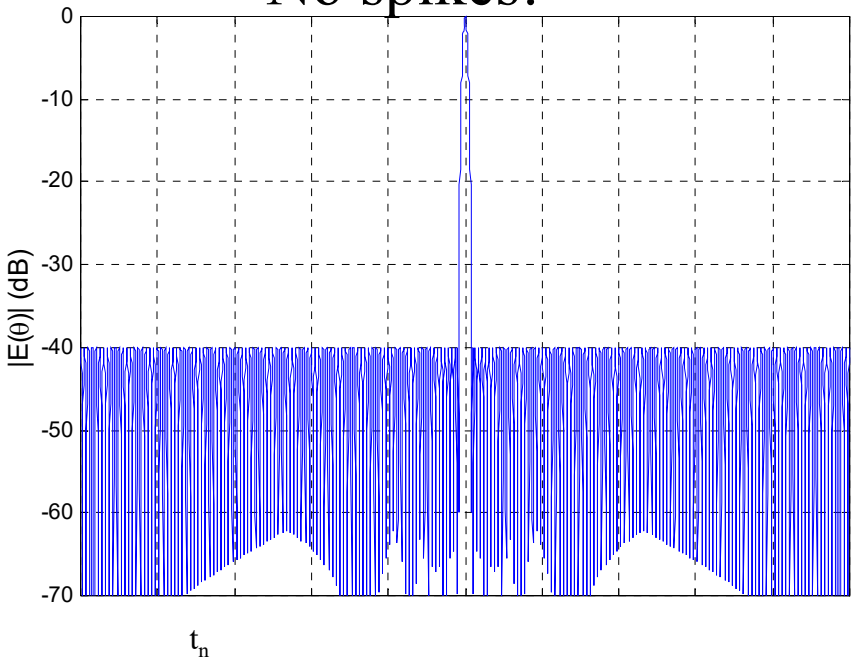

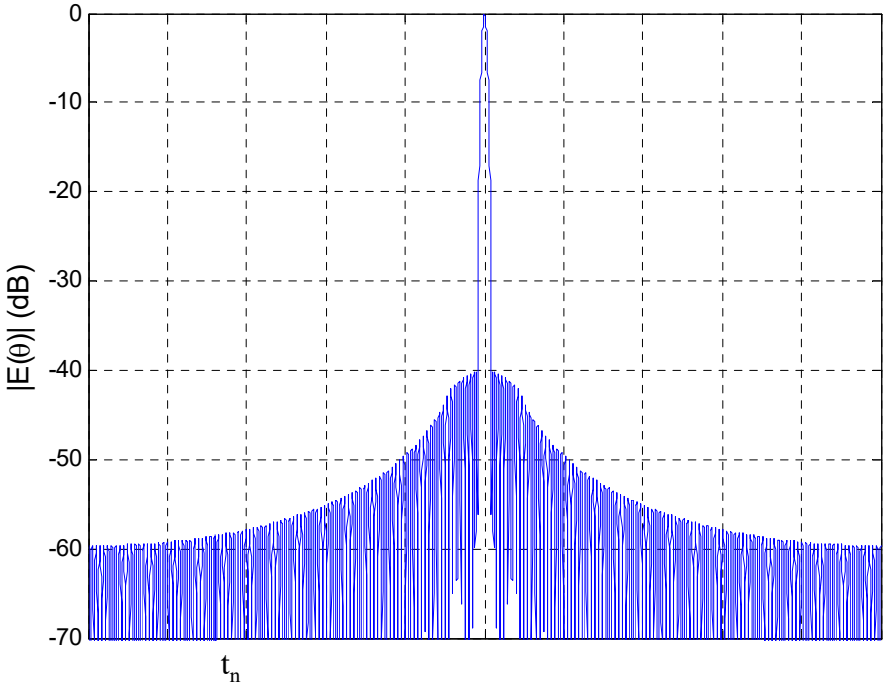

Chebyshev pattern -40dB

- Good approximation for the first SL
- SL asymptotic decay $\propto 1/x$
- Main beam widening
- n cannot be too small for an assigned SLR, but large n values yield implementation problems

Rete di Taylor: coefficienti

4. $w_{Tay}(t) = \sum_{m=-\infty}^{\infty} F_m \, w_0\left(t - \frac{m}{B}\right)$

where

$F_0 = 1$, $F_m = 0$ for $|m| \geq \bar{n}$

and

$F_m = F_{-m}$

TAYLOR WEIGHTING:

$$W_{Tay}(f) = W_0(f)\left[1 + 2\sum_{m=1}^{\bar{n}-1} F_m \cos 2\pi m \frac{f}{B}\right]$$

(REFS. 39,42,43)

TABLE 10.9 Taylor Coefficients F_m*

Design sidelobe ratio, dB	−30	−35	−40	−40	−45	−45	−50
$\bar{n}$	4	5	6	8	8	10	10
Main lobe width, −3 dB	1.13/*B*	1.19/*B*	1.25/*B*	1.25/*B*	1.31/*B*	1.31/*B*	1.36/*B*
F_1	0.292656	0.344350	0.389116	0.387560	0.428251	0.426796	0.462719
F_2	−0.157838(−1)	−0.151949(−1)	−0.945245(−2)	−0.954603(−2)	0.208399(−3)	−0.682067(−4)	0.126816(−1)
F_3	0.218104(−2)	0.427831(−2)	0.488172(−2)	0.470359(−2)	0.427022(−2)	0.420099(−2)	0.302744(−2)
F_4		−0.734551(−3)	−0.161019(−2)	−0.135350(−2)	−0.193234(−2)	−0.179997(−2)	−0.178566(−2)
F_5			0.347037(−3)	0.332979(−4)	0.740559(−3)	0.569438(−3)	0.884107(−3)
F_6				0.357716(−3)	−0.198534(−3)	0.380378(−5)	−0.382432(−3)
F_7				−0.290474(−3)	0.339759(−5)	−0.224597(−3)	0.121447(−3)
F_8						0.246265(−3)	−0.417574(−5)
F_9						−0.153486(−3)	−0.249574(−4)

*$F_0 = 1$; $F_{-m} = F_m$; floating decimal notation: −0.945245(−2) = −0.00945245.

Confronto reti di pesatura

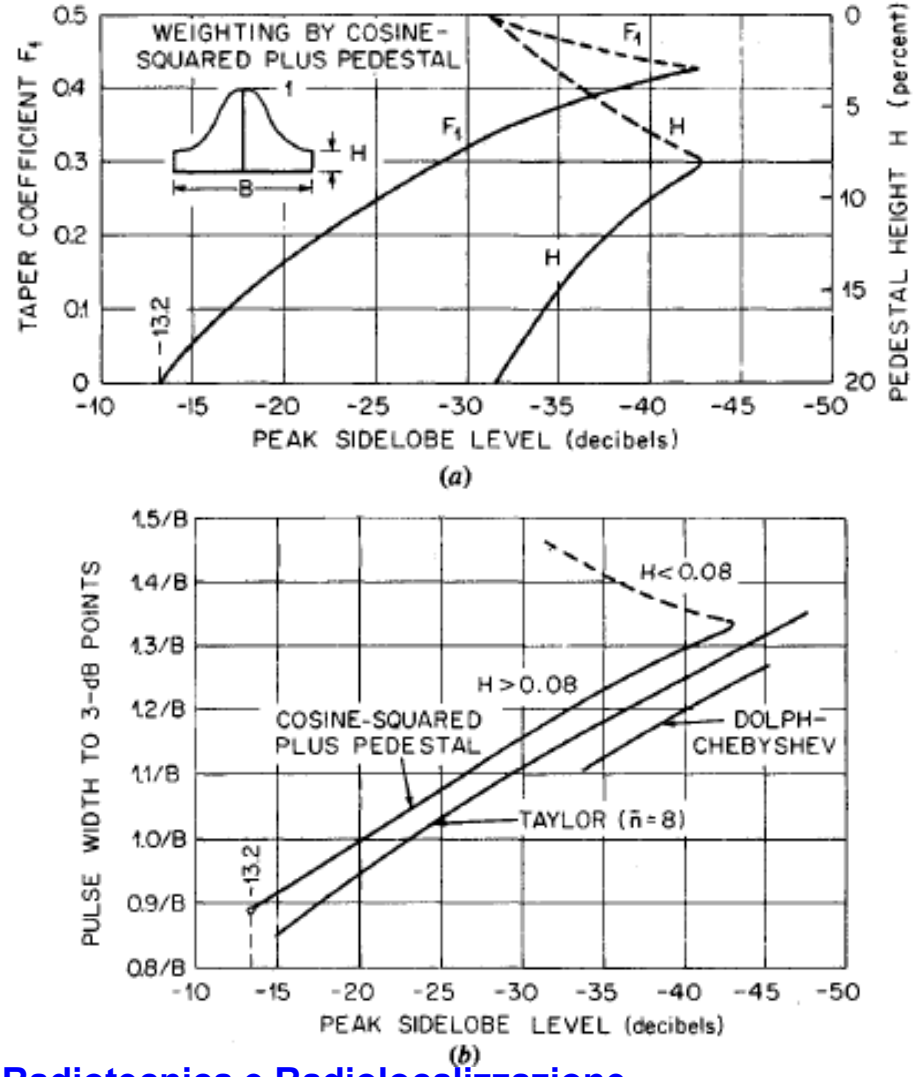

FIG. 10.16 (*a*) Taper coefficient and pedestal height versus peak sidelobe level. (*b*) Compressed-pulse width versus peak sidelobe level. (*c*) *SNR* loss versus peak sidelobe level.

Chirp approximation and sidelobes (II)

- **Side Lobe di Fresnel**

$$S.L.F.\big|_{dB} = 20\,\log(BT) + 3$$

Porzione trascurata nell'approx rettangolare

Importante per bassi rapporti di compressione

Limita la possibilità di abbassare i lobi laterali tramite pesatura